What is Trishear?

Alexander J. Coleman[1]*, Oliver B. Duffy[2] and Christopher A.-L. Jackson[1]

[1]*Basins Research Group (BRG), Department of Earth Science and Engineering, Imperial College, Prince Consort Road, London SW7 2BP, UK*

[2]*Bureau of Economic Geology, The University of Texas at Austin, University Station, Box X, Austin, Texas 78713-7508, USA*

**Corresponding author's e-mail: a.coleman14@imperial.ac.uk*

Abstract

The kinematics of fault-propagation folds, formed above the tips of upward propagating normal faults, is typically inferred from numerical and physical models. Trishear is a forward kinematic model in which deformation occurs in a triangular zone in front of the propagating fault tip, with the geometry of this zone, and the geometry and growth of the resulting fold, related to several parameters (e.g. fault dip, trishear angle, trishear symmetry, concentration factor, cover thickness). Trishear is powerful as it can model fold growth through time, allowing us to assess how natural structures identified in the field or in seismic reflection data evolved. However, the geological significance of trishear is poorly understood, and the effects of trishear parameters on the overall fold geometry and the stratigraphic architecture of synkinematic deposits remain poorly constrained. In this study we vary trishear parameters independently to demonstrate how they control the temporal variability in fold geometry and size, and how this is recorded in the architecture of synkinematic strata. We show that the propagation-to-slip ratio (the ratio between upper tip propagation into the cover and slip increment at the fault centre) is the most important factor in fold growth. When this ratio is relatively low, other parameters, such as the trishear angle and symmetry, concentration factor, more strongly control fold shape and size, with fault dip arguably and perhaps surprisingly being the least important. When this ratio is relatively high, the cover is breached rapidly, leaving little time for folding. Our analysis predicts that fault-propagation folds widen rapidly and establish their near-final width early during fold growth, whereas fold amplitude develops gradually with fault slip. Fold shape therefore significantly changes throughout fold growth. During early fold growth, folds are wide with initially small amplitudes but gradually amplify as folding progresses so that

amplitudes and widths become increasingly similar towards the later stages of growth folding, folds have similar widths but have large amplitudes. We also speculate on the geological significance of the propagation-to-slip ratio, trishear angle, concentration factor and trishear symmetry, and under what scenarios these parameters may correspond to in extensional basins. Our results have implications for understanding the geometry and growth of extensional fault-propagation folds, and for estimating the best-fit parameters (and related geological controls) for natural examples.

Introduction

Extensional fault-propagation folds form above the tips of upward-propagating normal faults (e.g. Horsfield, 1977; Withjack et al., 1989; Withjack et al., 1990; Gawthorpe et al., 1997; Lewis et al., 2015; Fig. 1). These folds are characterised by an upward widening zone of ductile deformation above a discrete, brittle fault at depth (e.g. Hardy and Ford, 1997; Allmendinger, 1998; Hardy and McClay, 1999; Withjack and Callaway, 2000). Our understanding of how these folds grow comes from: (1) field (e.g. Gawthorpe et al., 1997; Sharp et al., 2000a; Sharp et al., 2000b; Khalil and McClay, 2002; Lewis et al., 2015; Khalil and McClay, 2016; Fig. 2E - F) and seismic reflection studies (e.g. Pascoe et al., 1999; Corfield and Sharp, 2000; Corfield et al., 2001; Ford et al., 2007; Marsh et al., 2010; Jackson et al., 2017; Tavani et al., 2018; Fig. 2C - D), where synkinematic strata permit rare glimpses into their geometric and kinematic evolution, or (2) inverse models, where the best-fit kinematic parameters for specific fold geometries may be estimated (e.g. Allmendinger, 1998; Cardozo et al., 2003; Allmendinger et al., 2004; Cardozo et al., 2011). Physical models (e.g. Horsfield, 1977; Withjack et al., 1989; Withjack et al., 1990; Withjack and Callaway, 2000; Fig. 2A) and forward numerical models (Erslev, 1991; Hardy and Ford, 1997; Allmendinger, 1998; Zehnder and Allmendinger, 2000; Cardozo et al., 2003; Patton, 2004; Cardozo et al., 2011; Fig. 2B) allow us to track fault-fold growth through time, and to explore how fault- (e.g. dip, depth of nucleation) and material-related (e.g. propagation-to-slip ratio, trishear angle) parameters control fold shape and kinematics.

Although physical and forward numerical models have provided important insights as to the controls of and strain within extensional fault-propagation folds, their geometry through time is rarely quantified or systematically explored, limiting their application to natural examples. Furthermore, the geological significance of many of the parameters used in forward numerical models is rarely considered; for example, what aspect of the geology dictates trishear angle or propagation-to-slip ratio (cf. Hardy and McClay, 1999)? Because of this, our understanding of how fault-propagation folds grow through time is limited, and how this is recorded in the architecture of synkinematic growth strata is poorly constrained. These first-order unknowns have important implications for how we structurally restore extensional forced-folds (cf. Lingrey and Vidal-Royo, 2015), and for our understanding of what key geological parameters controls fold geometry through time and, therefore, where such structures may best develop (cf. Allmendinger, 1998; Ford et al., 2007; Conneally et al., 2017).

Here, we use FaultFold©, a kinematic trishear model (Hardy and Ford, 1997; Allmendinger, 1998; Zehnder and Allmendinger, 2000), to investigate how trishear parameters affect the geometric evolution of fault-propagation folds and their associated growth strata. While previous studies have used trishear models on individual folds to constrain the trishear parameters responsible for their geometry, size and evolution (Table 1), there have been few attempts to systematically understand how each trishear parameter affects fold geometry and synkinematic architecture through time, and their geological significance. This has made it difficult to compare trishear models to mechanical (e.g. Johnson and Johnson, 2002; Finch et al., 2004; Hardy, 2011) or physical models (e.g. Horsfield, 1977; Withjack et al., 1990; Miller and Mitra, 2011), and to understand the geometric and kinematic differences between them. By isolating trishear parameters in a series of fault-propagation fold forward models, we investigate: (i) the controls the geometry and size of fault-propagation folds during their growth, (ii) how trishear parameters may correlate to the physical properties of natural rock, and (iii) the limitations of trishear in evaluating the geometry and growth of fault-propagation folds. Our results allow us to compare trishear predictions with physical and numerical models, and with natural examples in Chapter 5.

Kinematics of trishear deformation

Field, seismic reflection, and physical modelling studies show blind normal faults are often overlain by upward widening zones of distributed deformation or folding (Fig. 1). Blind propagating normal faults are essentially large mode II cracks (Allmendinger, 1998), with theoretical studies of such cracks indicating they are related to broadly triangular zones of high stress, with these zones attached to and widening out from their tips (e.g. Pollard and Segall, 1987; Crider et al., 1996). This triangular zone is geometrically reminiscent of trishear models (Erslev, 1991; Allmendinger, 1998), where a zone of distributed shearing and enhanced deformation is attached to the fault tip ('trishear zone'; Hardy and Ford, 1997; Fig. 3).

The trishear zone, with angles ϕ_{FW} and ϕ_{HW}, lies between two rigid, undeformed zones near the upper fault tip. Outside of the trishear zone and within the hangingwall and footwall, constant velocity fields are assigned, while in the trishear zone itself, velocity varies. In the hangingwall, above the fault, material moves as a rigid body in the direction of fault slip. In the footwall, below the fault, the material is also rigid but is stationary (Fig. 3).

As the footwall and hangingwall blocks move relative to one-another, the cover material above the blocks and in the trishear zone deforms, becoming folded. Within the trishear zone, the cross-sectional area of the rock does not change (Equation 1; Waltham and Hardy, 1995), and material does not move in or out of the section. Instead, all material movement is strictly in-plane, as is often assumed during structural restoration (e.g. Hossack, 1979; Rowan and Kligfield, 1989; Erslev, 1991; Wickham and Moeckel, 1997; Lingrey and Vidal-Royo, 2015). The velocity normal to the fault plane at the boundary between the hangingwall and the trishear zone is zero (Vy = 0 on Fig. 3; Equation 2; Hardy and Ford, 1997). The velocity parallel to the fault is equal to the fault slip velocity (Vx = V0 on Fig. 3; Equation 2; Zehnder and Allmendinger, 2000). As the footwall does not move, velocities normal and parallel to the fault plane are zero (Equation 3; Zehnder and Allmendinger, 2000). The velocity within trishear zone therefore decreases linearly from the hangingwall to the footwall to conserve area, which in practical terms is numerically handled by splitting the trishear zone into multiple sectors (Equation 4; Hardy and Ford, 1997), starting at the fault tip and extending into the cover in the direction of fault propagation (i.e. the x-direction on Fig. 3). The trishear zone may also be divided into sectors in the direction normal to the fault plane (i.e. the y-direction on Fig. 3), allowing the slip vector at a particular point in the trishear zone to vary. Furthermore, the trishear zone may be asymmetric and still conserve the cross-sectional area of the rock (Zehnder and Allmendinger, 2000; Johnson and Johnson, 2002; Zhao et al., 2017). Because the direction of shear within the trishear zone is often oblique to the stratal layering, the layers change in thickness as they pass through the trishear zone, even if the cross-sectional area of the rock is conserved.

Equation 1:

$$\frac{\partial v_x}{\partial x} + \frac{\partial v_y}{\partial y} = 0$$

$where\ \frac{\partial v_x}{\partial x} = change\ in\ fault\ slip\ velocity\ in\ the\ x\ direction\ with\ respect\ to\ x,$

$\frac{\partial v_y}{\partial y} = change\ in\ the\ fault\ slip\ velocity\ in\ the\ y\ direction\ with\ respect\ to\ y$

Equation 2:

$$v_x = v_0,\ v_y = 0,\ \text{where } y = x\tan(\phi_{HW})$$

where v_x = the velocity in the x direction (parallel to the fault plane),
v_y = the fault slip velocity in the y direction (perpendicular to the fault plane),
v_0 = the known fault slip velocity in the hangingwall,
ϕ_{HW} = the angle of the trishear angle in the hangingwall

Equation 3:

$$v_x = v_y = 0,\ \text{where } y = -x\tan(\phi_{FW})$$

where v_x = the velocity in the x direction (parallel to the fault plane),
v_y = the fault slip velocity in the y direction (perpendicular to the fault plane),
v_0 = the known fault slip velocity in the hangingwall,
ϕ_{FW} = the component of the trishear angle in the hangingwall

Equation 4:

$$(v_x)_i = v_i\cos(\phi_i)\,,(v_y)_i = -v_i\sin(\phi_i)$$

where $(v_x)_i$ = the fault slip velocity in the x direction for the ith section,
$(v_y)_i$ = the fault slip velocity in the y direction for the ith section,
v_i = the fault slip velocity in the ith section,
ϕ_i = direction of the fault slip in the ith section

The angle of the trishear zone (ϕ), the velocities normal (v_x) and parallel (v_y) to the fault plane, and the fault slip velocity (v_0) may vary. As the fault slips, its upper tip may propagate into the cover and its related trishear zone, the rate of which is controlled by the propagation-to-slip (P/S) ratio. As the fault propagates through the cover, the trishear zone moves with it and at a rate that is independent of the fault slip (Hardy and Ford, 1997). As velocity within the trishear zone does not have to be linear or homogeneous to conserve cross-sectional rock area (Zehnder and Allmendinger, 2000), the concentration factor (CF), which controls the velocity distribution in the trishear zone, may also be varied. Where trishear is homogeneous or linear (CF ~ 1), rocks are rotated uniformly, perpendicular to the fault plane. Where trishear is heterogeneous or non-linear (CF $\neq$ 1), rocks in the centre of the trishear zone are rotated to a greater degree than those near the edges (Zehnder and Allmendinger, 2000; Johnson and Johnson, 2002). As the trishear zone does not have to be symmetrical to conserve cross-sectional area (Zehnder and Allmendinger, 2000), the degree of trishear symmetry may also be varied. Rocks entering the trishear zone are not limited to the prekinematic strata. As synkinematic strata are deposited atop the growing fold, portions within the trishear zone may also be folded or at least displaced by the propagating fault tip.

There are an infinite number of kinematic motions within the trishear zone that may conserve cross-sectional rock area (Zehnder and Allmendinger, 2000), thus understanding the most important trishear parameters and their mechanical significance is paramount for understanding how folds grow. To date, only very few attempts (Khalil and McClay, 2002; Ford et al., 2007; Jin et al., 2009; Conneally et al., 2017) have been made to relate changes in fold geometry with time to trishear parameters. By forward modelling fault-propagation fold geometries and their synkinematic strata, we may be able to predict characteristic fold shapes associated with particular trishear parameters so that they may be related to geological features and factors in nature, but which may shed light on how fault-propagation folds grow. Importantly, these trishear models are purely conceptual, but by varying their parameters, we may be able to compare their geometrical predictions for fault-propagations with natural examples to find reasonable parameter values and bounds, and to speculate on their geological significance.

Trishear parameters and model setup

During trishear modelling, various parameters (see Figs. 4 – 5 for definitions) may be changed at any time during the model run. These parameters are associated with the stratigraphy (e.g. prekinematic and synkinematic thickness), the fault (e.g. geometry, dip, throw), and the trishear zone itself (e.g. concentration factor, trishear symmetry, trishear angle, the propagation-to-slip ratio). In the forward models, the nature and location of deformation during fault slip is controlled by the trishear apical angle, the propagation-to-slip ratio, the concentration factor, and the degree of trishear symmetry. The apical angle controls the width of the deformation above the fault tip, whereas the P/S ratio controls how rapidly the fault tip and the trishear zone propagates through the cover (Hardy and Ford, 1997; Allmendinger, 1998; Zehnder and Allmendinger, 2000; Hardy and Allmendinger, 2011; Zhao et al., 2017). The concentration factor controls the intensity, location and focus of deformation within the trishear zone, whereas the trishear symmetry controls whether shear is focused towards the hangingwall or footwall (Zehnder and Allmendinger, 2000).

Although all of the aforementioned trishear parameters may change in the trishear model, only some may plausibly change in nature. For example, we speculate that the P/S ratio may change due to the rheology of the host rock (cf. Couples et al., 1998; d'Alessio and Martel, 2004), the depth in the crust at which deformation occurs (Hardy and Ford, 1997), and the regional strain rate (cf. Nicol et al., 1997; Hardy and McClay, 1999; Meyer et al., 2002; Mueller, 2017). Similarly, the apical angle is likely a function of the cover strength (Allmendinger, 1998) or strain hardening (Conneally et al., 2017), both of which may relate to how localised strain becomes as a function of host rock rheology. Although concentration factor is also likely related to the cover rheology (as it controls the intensity, position and focus of deformation within the trishear zone), the geological significance of this parameter is poorly constrained.

In the forward models presented here, only one parameter was varied at a time to investigate its effect on fault-propagation fold geometry and the architecture of synkinematic strata (see Table 2). The initial model included a sequence of isopachous, prekinematic layers with a fault tip at its base. Although the trishear model is dimensionless, individual parameters are scaled relative to one-another (e.g. slip increment is scaled to the layer thickness). Normal fault throw increased during the model run at a constant rate, with the geometry of the overlying fold measured at each step (see Fig. 4). Once the fold within the prekinematic cover was breached, we stopped the model, and no further measurements were recorded for fold geometry. In all cases, synkinematic strata was deposited atop the growing fold at regular fault throw increments such that any fold-related accommodation was filled and no at-surface structural relief developed. Furthermore, our models did not incorporate erosion of pre- or synkinematic strata. In this way, growth strata record the strain and the complete geometric development of the fault-propagation fold. The thickness of the synkinematic strata and the width of lateral thinning were then recorded throughout the model run (see Fig. 5). For simplicity, when describing the fold shape, we define the ratio of the fold width to fold amplitude as the ‘fold-shape-factor’ (FSF). When fold width is greater than fold amplitude, FSF > 1; when fold width and amplitude are the same, FSF ~ 1; when fold width is less than fold amplitude, FSF < 1. See Fig. 6 for a summary of the trishear modelling results.

The effects of trishear on fold geometry

In this section we describe how the cover thickness, fault dip, P/S ratio, trishear angle, concentration factor and symmetry of the trishear zone within the trishear model is predicted to affect fault-propagation fold geometry.

Cover thickness

Variations in cover thickness reflect the depth of fault nucleation. Low cover thicknesses are likely when the fault nucleates at shallow depths, whereas high cover thicknesses are indicative of when the fault nucleates at greater depths. As cover thickness increases above a propagating normal fault, the duration of folding increases as there is a larger amount of rock above the upper fault tip. Given the greater duration of folding (cf. Williams and Chapman, 1983; Johnson and Johnson, 2002), greater cover thicknesses are associated with wider and higher amplitude folds (Fig. 6A). In addition, as cover thickness increases, the width of the fault-propagation fold increases (Fig. 7). Fold width is established very early and remains largely constant, irrespective of cover thickness. Fold amplitude does not change for a given cover thickness and gradually increases with increasing fault throw. In all cases, the FSF decreases with ongoing fault slip. This is because fold width is established early during fault slip while the amplitude is still relatively small, but with continued fault slip, amplitude increases while width does not significantly change. As fold width is significantly larger for thicker cover thicknesses, the initial FSF is also larger. Finally, as the cover thickness increases, the dip of the fold limb decreases for a given fault throw. This is because the top of the fault-propagation fold is further away from the propagating fault tip for a thick rather than thin cover.

Fault dip

Variations in fault dip may be controlled by the lithology of the hosting strata, its depth, the presence of pre-existing structures (Barnett et al., 1987; Walsh and Watterson, 1988; Pei et al., 2014), but how fault dip impacts the geometry and size of folds developed at their upper tips has largely been investigated using physical models (Tsuneishi, 1978; Withjack et al., 1990; Withjack and Callaway, 2000) but rarely quantified. As fault dip decreases, the duration of folding increases as there is a larger volume of rock ahead of the upper fault tip. Furthermore, shallowly-dipping faults are capable of generating larger folds compared to steeply-dipping faults because the latter breach the surface more rapidly (Fig. 6B), similar to observations in physical models (Horsfield, 1977; Withjack et al., 1990). The fold amplitude increases gradually and at the same rate as increasing fault throw. However, shallowly-dipping faults take longer to reach large fold amplitudes (Fig. 8A_1 - A_4) compared to steeply-dipping faults (Fig. 8B_1 - B_4), as a greater amount of displacement is accommodated as heave on shallowly-dipping faults, as opposed to throw (which controls fold amplitude) on steeply-dipping faults. Moreover, shallowly-dipping faults may reach similar fold amplitudes as their steeply-dipping counterparts, but much later during fold growth. As fault dip increases, the width of the associated fault-propagation fold decreases. Irrespective of fault dip, the near-final fold width is established very rapidly during fold growth (Fig. 8), in contrast to the fold amplitude. After an initial phase of rapid widening, fold width increases very slowly with increasing fault throw, similar to that observed in mechanical models (cf. Finch et al., 2004; Hardy, 2011; e.g. Smart and Ferrill, 2018). As fold amplitude and width develop at different rates as a function of the fault dip, the FSF may be significantly different between steeply- and shallowly-dipping faults (Fig. 6B). Overall, the FSF decreases with ongoing fault throw regardless of fault dip, although shallow faults have higher FSF values compared to steep faults (Fig. 8). The fold limb dip progressively increases with ongoing fault throw, however, steeply-dipping faults are associated with steeply-dipping fold limbs (Fig. 8B), whereas shallowly-dipping faults are associated with shallowly-dipping fold limbs (Fig. 8A).

Our trishear analysis suggests fold width is established relatively early during deformation, similar to physical (e.g. Withjack et al., 1990) and mechanical models (e.g. Finch et al., 2004; Hardy, 2011, 2013; Smart and Ferrill, 2018). We also show that fault dip strongly affects fold shape and particularly, how rapidly the width or amplitude develops. Numerical models from Patton (2004) suggested that fault dip is only important at relatively shallow depths when the fault is buried by a thin veneer of prekinematic strata (cf. Fig. 3 in Patton, 2004). In contrast, the forward models here and the published physical models suggest that the fold width and amplitude are influenced by fault dip even if covered by relatively thick cover (cf. Fig. 7B). However, in the forward models presented here and in published physical models (e.g. Withjack et al., 1990), the fault may be regarded as relatively shallowly buried.

Propagation-to-slip (P/S) ratio

The geological significance of the P/S ratio is poorly understood. Previous studies have interpreted the P/S ratio as related to the rheology of the overburden (Hardy and Ford, 1997;

Allmendinger, 1998) and the regional strain rate (Hardy and Ford, 1997; Hardy and McClay, 1999). Where the P/S ratio is high, the cover is thought to be relatively strong and homogeneous while low P/S ratios have been associated with relatively weak, heterogeneous cover (Hardy and Finch, 2006, 2007). Where the regional strain rate is high, the P/S ratio of the faults (if strain was distributed equally across the array) may be expected to also be high (cf. Hardy and Ford, 1997; Hardy and McClay, 1999). In addition, we speculate that the P/S may also reflect strain localisation in rifts (cf. Cowie et al., 2005) and early vs. late rift phases (cf. Cowie, 1998; Gupta et al., 1999; Gawthorpe and Leeder, 2000), where an increase in slip rate and strain localisation may promote rapid upper fault tip propagation (and hence higher P/S ratios) on large, mature faults towards the rift axis, although these remain untested. Whatever its significance, folds associated with high P/S values are breached earlier than those with low P/S values (Fig. 9), similar to prior studies (Hardy and Ford, 1997; Allmendinger, 1998; Khalil and McClay, 2002; Allmendinger et al., 2004; Jin et al., 2009; Welch et al., 2009; Pei et al., 2014; Zhao et al., 2017). As the P/S ratio increases, the duration of folding decreases. Furthermore, low P/S ratios are associated with larger folds and lower FSFs (Fig. 6C), largely because the near-final fold width (regardless of the P/S value) is established relatively early during fold growth, while amplitude develops gradually. As folds associated with high P/S values are breached relatively early compared to those associated with low P/S values, and so the maximum dip of the fold limb before breaching is lower for a high P/S ratio (e.g. Figs. 5 - 6 in Hardy and McClay, 1999).

Trishear angle

Variations in trishear angle likely reflect the rheology of the deforming rock mass. More specifically, large trishear angles may reflect relatively wide zones of deformation that may be expected in relatively weak strata, whereas narrow trishear angles likely reflect localised, intense deformation in strong, brittle cover strata (Allmendinger, 1998; Hardy and Finch, 2007; Conneally et al., 2017). As trishear angles likely reflect the rheology of the cover, they may be also intimately related to the P/S ratio (cf. Jackson et al., 2006). In other words, where the cover is ductile and weak, the trishear angle is large but the P/S is low, whereas brittle, strong cover is associated with a small trishear angle and high P/S ratio.

Trishear angle strongly controls fold geometry (Fig. 6D; cf. Allmendinger, 1998; Allmendinger et al., 2004). As the trishear angle is increased, so does the fold width (Fig. 10), which is established rapidly and early in the fold evolution similar to the trishear models of Hardy and McClay (1999; in their Fig. 3), and the physical models of, for example, Withjack et al. (1990;

in their Figs. 4, 6 and 7). The fold amplitude, in contrast to the width, is unaffected by the trishear angle and simply increases with increasing fault throw. As trishear angles affect fold width, but not the fold amplitude, high FSF values are associated with larger trishear angles. Regardless of the trishear angle, the FSF decreases with increasing fault throw. For a given fault throw, folds associated with large trishear angles have steeper fold dips, whereas folds with small trishear angles are breached before the dipping fold limb becomes steep. Folds associated with small trishear angles do not reach the steep limb dips or low FSF values typically associated with large trishear angles. This is because they are breached relatively early during fold evolution, compared to folds with large trishear angles, which are breached relatively late and only at high throws.

Concentration factor (CF)

Similar to the trishear angle, the mechanical significance of concentration factor and its relation to natural examples is still poorly understood. However, given that it describes the intensity, position and focus of deformation in the trishear zone, it might also be related in some way to the rheology of the cover (cf. Zehnder and Allmendinger, 2000). However, in contrast to the P/S ratio and trishear angle, the geological significance of the concentration factor, and its reasonable bounds in nature, have not been explored. Linear velocity fields (CF ~ 1) are characterised by a single, smooth and broad fold (Fig. 6E) while non-linear velocity fields (CF $\neq$ 1) are characterised by either double fold hinges (cf. A_1 – A_3 in Fig. 11) at very low concentration factors (CF << 1) that dissipates with ongoing deformation (cf. A_4 in Fig. 11), or negligible folding at very high concentration factors (CF >> 1; Fig. 6E). Fold width is strongly controlled by concentration factor; at low, non-linear or at linear concentrations factors (i.e. ≤ 1), folds are wide, whereas at high, non-linear concentration factors (i.e. >> 1), folds are narrower and poorly-developed (Fig. 11). Regardless of the concentration factor, if a fold develops, the fold width is established early during deformation. In contrast, fold amplitude is not affected by the concentration factor, and again simply increases with increasing fault throw. Given fold width is dependent on the concentration factor but amplitude is not, low non-linear and linear concentration factor (i.e. ≤ 1) folds are associated with high FSF values whereas relatively high concentration factor (i.e. > 1) folds are associated with low FSF values. Irrespective of the concentration factor, the FSF value decreases with increasing fault throw (Fig. 11). At low non-linear or linear concentration factors (i.e. ≤ 1), the dip of the fold limb does not significantly change (cf. Fig. 11). However, very high concentration factors (i.e. >> 1), as shown in Fig. 6E, generate almost no folding and thus, where folds are present, they are very narrow and have steeply-dipping fold limbs or appear similar to block faulting (cf. Jin and Groshong, 2006). In contrast, low non-linear concentration factors (i.e. < 1) may even produce multiple fold hinges associated with each edge of the trishear zone (A_1 - A_3 in Fig. 11), as shown by Zehnder and Allmendinger (2000; in their Figs. 4 and 6).

Trishear symmetry

The symmetry of the trishear zone describes how strain is distributed in the vicinity of the propagating fault tip (Fig. 6F). In natural examples and physical models, the trishear zone is rarely symmetrical (e.g. Jin and Groshong, 2006; Ford et al., 2007; Jin et al., 2009) and is often focused towards the hangingwall or footwall (Table 2). Although what controls the degree and direction of trishear asymmetry is also poorly understood, it might be related lithological changes across the fault, or potentially strain hardening. For example, if salt is largely present in only the hangingwall (e.g. Figs. 5C and 10C in Lewis et al., 2013; Fig. 2D in Jackson and Lewis, 2013), folding may preferentially focused towards the footwall side.

Asymmetric shear that is focused towards one side of the fault, towards the hangingwall for example, is typically associated with negligible degrees of folding (A_1 – A_4 in Fig. 12). Furthermore, fault-propagation folds associated with symmetrical trishear (B_1 – B_4 in Fig. 12) are generally larger, as they continue to grow for longer periods and remain intact for longer than their asymmetrical counterparts. Where the trishear zone is asymmetric, but only slightly focused towards one side of the fault (e.g. 60% towards the hangingwall; Ford et al., 2007; cf. Table 1), the degree of folding is similarly focused towards that side. Although fold amplitude is not affected by trishear symmetry and is instead, like the other models, related to fault throw, folds associated with symmetrical trishear are better developed and wider than their asymmetrical counterparts. Symmetrical trishear leads to wide folds that establish their width relatively early during fold growth (B_1 – B_4 in Fig. 12), whereas asymmetrical folds are very narrow (A_1 – A_4 in Fig. 12). Folds with symmetrical trishear are also typically associated shallowly dipping fold limbs compared to folds with asymmetrical trishear. In addition, FSF values for symmetrical shear scenarios decrease with ongoing fault slip. In contrast, asymmetric shear leads to complex FSF values, where FSF values initially increase and then decrease.

Predictions of fault-propagation fold shape, size and growth

Having forward modelled the fold geometry for each of the trishear parameters, we summarise which factors control the amplitude, width and shape of the fold, as well as those that control when the fold is breached and the dip of the fold limb (Fig. 6). By systematically describing the fold geometry and evolution, our results may permit a more detailed and considered application of the trishear kinematic model to natural examples. Fold amplitude is unrelated to any of the trishear parameters, instead simply increasing in concert with fault throw. In contrast, the fold width is highly dependent on the trishear parameters. Wide folds are associated with thick cover, shallowly-dipping faults, low P/S ratios, high trishear angles, low non-linear or linear concentration factors, and symmetrical trishear. In contrast, narrow folds are associated with thin cover, steeply-dipping faults, high P/S ratios, small trishear angles, high non-linear concentration factors, and asymmetrical trishear. Although fold width does increase with increasing fault throw, width is established early during fold growth. As the fault heave is less than the fold throw for a given displacement on steeply-dipping normal faults, fold width is established early and then slowly increases with fault heave. In contrast, fault throw is accrued gradually and thus, fold amplitude increases at a similar rate to fault throw. Given that fold amplitude develops gradually, while fold width is established early, FSF decreases with ongoing fault slip. Moreover, FSFs are initially large but exponentially decrease to smaller values in the latter stages of fold growth (cf. FSF on Figs. 7 – 12). In other words, folds are initially wide with small amplitudes but with increasing throw on the underlying normal fault, the fold amplifies at a greater rate than it widens. The only exception is likely to be where the fault dip is $< 45°$, as the heave would be greater than the throw for a given displacement on a shallowly-dipping normal fault.

The point the propagating fault tip breaches the surface is dependent on the amount of rock ahead of the propagating fault tip, how quickly the tip propagates through the cover, and the manner in which deformation is distributed. Folds associated with thin cover and steeply-dipping faults are breached relatively rapidly as the amount of rock in front of the tip is less than that in a setting characterised by thick cover and shallowly-dipping faults. High P/S ratios mean that there is only a short amount of time before the fold is breached, with high throws also associated with fold breaching. Low trishear angles, very high concentration factors, and asymmetrical trishear all lead to very narrow, intense zones of deformation focused above the propagating fault tip, a situation leading to rapid breaching of the fold. In contrast, more protracted folding is associated with thick cover, shallowly-dipping faults, low P/S ratios, high trishear angles, low concentration factors, symmetrical shear and low fault throws.

Synkinematic architecture

Fault-propagation folds have a marked impact on the distribution and architecture of synkinematic strata (Gawthorpe et al., 1997; Corfield and Sharp, 2000; Corfield et al., 2001; Gawthorpe and Hardy, 2002; Patton, 2004; Lewis et al., 2015). In the prior section, we used kinematic models to show how trishear parameters (see Fig. 4) affected the duration of folding (and timing of fold breaching), and fold geometry and size through time (see Fig. 6 for a summary). Here, we discuss how these same trishear parameters may affect the architecture of the synkinematic strata in response to fold growth so that particular parameters may be related to natural examples. In all cases, we assumed that sedimentation rate equalled or exceeded the rate of fold amplification, filling the available accommodation without being subjected to erosion (cf. Hardy and Ford, 1997). In all cases, synkinematic strata thin and onlap onto the fold hinge and thicken basinwards until the fold is breached. For simplicity, we define 'fold-related accommodation' as periods when the fold has not been breached (Fig. 2E – F; cf. Fig. 3A in Gawthorpe et al., 1997), and 'fault-related accommodation' as periods when the fold has been breached and the fault tip has reached the surface (Fig. 2C – D; cf. Fig. 3B in Gawthorpe et al., 1997). For each parameter and throughout fold growth, the footwall to hangingwall (HW:FW) thickness and the width of stratal thinning were also measured (Fig. 5).

Increased prekinematic cover thicknesses generate wide fault-propagation folds and are thus associated with wider zones of synkinematic stratigraphic thinning (Fig. 13A). In contrast, thin prekinematic cover thicknesses are associated with narrow folds and narrow zones of stratigraphic thinning. The HW:FW thickness, irrespective of the cover thickness, is largely similar. Given that thick cover also promotes longer periods of folding compared to thin cover, increased prekinematic cover thickness are associated with prolonged periods of fold-related accommodation and a relatively late and minor phase of fault-related accommodation generation (Fig. 6A). Conversely, thin prekinematic cover thicknesses are associated with relatively early breaching of the fold and therefore, only a short phase of fold-related accommodation.

For a given throw, shallowly-dipping faults are associated with broader folds compared to steeply-dipping faults (Fig. 6B). Furthermore, for a given fault throw, synkinematic strata associated with folds underlain by shallow faults have much larger widths of thinning, and are associated with decreased HW:FW thickness ratios compared to folds underlain by steep faults

(Fig. 13B). Similar to the prekinematic thickness variations, as shallowly-dipping faults breach folds relatively late in the deformation history, fold-related accommodation is likely to dominate the synkinematic architecture. In contrast, steeply-dipping faults may have some fold-related accommodation during the early part of fault slip and fold growth, but the fold is likely to be breached relatively rapidly. Furthermore, fault-related accommodation likely dominates the synkinematic succession.

The propagation-to-slip ratio fundamentally controls the duration of folding. As high P/S ratios lead to early breaching of the overlying fault-propagation folds, the fold-related accommodation phase is relatively short-lived and therefore, thin fold-related synkinematic wedges develop. Conversely, high P/S ratios are associated with thicker sequences of fault-related synkinematic wedges (Fig. 6C). Given the rapid breaching of the fold under high P/S conditions, folding is not well-developed, and therefore, the width of zone of synkinematic stratigraphic thinning towards the fold is relatively narrow. The HW:FW thickness is largely similar for high and low P/S ratios (Fig. 13C).

The trishear angle does not affect the thickness of the synkinematic strata in the footwall versus the hangingwall. However, given large trishear angles lead to broader folds, the width of synkinematic thinning increases with larger trishear angles (Fig. 13D). In contrast, small trishear angles lead to narrow folds and thus, synkinematic strata thin over a relatively narrow zone. In extreme cases, where the trishear angle is very small and strain is focused immediately above the propagating fault tip, the width of synkinematic thinning is also very narrow. Where the width of thinning is very small (less than a few 10s of metres), it may not be resolvable in seismic reflection data (cf. Botter et al., 2014).

Variations in the concentration factor do not affect the HW:FW thickness ratio (Fig. 13E). However, high non-linear concentration factors (i.e. CF > 1) are associated with very narrow fold widths (Fig. 6E). Therefore, very abrupt across-fault thickening, associated with very narrow synkinematic thinning widths, preferentially develop with high concentration factors (Fig. 13E). Low non-linear or linear concentration factors (i.e. CF $\leq$ 1) in contrast, are characterised by large widths of synkinematic thinning. High concentration factors also lead to very early fold breaching during extension and look similar to block faulting; synkinematic wedges are therefore associated with fold-related accommodation are typically very thin and only form during the very early stages of extension. Instead, synkinematic successions are related to fault-related accommodation phases. In nature, this might mean that the early fold-related accommodation phase may not be captured in the architecture of synkinematic strata. In contrast, low non-linear or linear concentration factors (i.e. CF ≤ 1) are associated with broad zones of synkinematic thinning and are breached relatively late during extension. In some cases, multiple fold hinges develop ($A_1 – A_3$ in Fig. 11) within the trishear zone, creating complex onlap patterns (Fig. 14).

When trishear deformation is preferentially focused towards one side of the fault and shear is asymmetric, the geometry of synkinematic strata significantly changes (Fig. 6F). For example, when strain is asymmetric and focused towards the hangingwall, the fault-propagation fold is breached relatively early during deformation, and the geometry of related synkinematic strata is controlled by fault- rather than fold-related accommodation ($A_1 – A_4$ in Fig. 12). If the strain is symmetric, the fold is well-developed and breached relatively late during extension ($B_1 – B_4$ in Fig. 12). In response, and in comparison to the case of asymmetric shear, synkinematic strata thins over a wider region onto a symmetric fold (Fig. 13F) and is dominated by fold-related synkinematic wedges. The HW:FW ratio is similar regardless of the asymmetric shear (Fig. 13F).

Discussion

What controls the geometry and size of fault-propagation folds during their growth?

The growth of fault-propagation folds has implications for structural restorations in areas of extension (e.g. Lingrey and Vidal-Royo, 2015), the tectono-stratigraphic development of rifts (e.g. Gawthorpe and Leeder, 2000; Sharp et al., 2000a; Sharp et al., 2000b; Jackson et al., 2006), and the distribution and geometry of synkinematic hydrocarbon reservoirs (Lewis et al., 2015). However, the growth of fault-propagation folds, in terms of their size and shape, is rarely quantified or systematically explored.

Prior studies show that the geometry, size and occurrence of fault-propagation folds in nature and in models may be related to particular trishear parameters; however, the relative importance of these parameters is poorly constrained (Hardy and Ford, 1997; Allmendinger, 1998; Hardy et al., 1999; Allmendinger et al., 2004; Jin and Groshong, 2006; Hardy and Allmendinger, 2011). By using forward kinematic models, we have identified how each trishear parameter affects not only the fold growth, but also its geometry and size with ongoing fault slip, and thus, the synkinematic architecture. Our trishear results predict that fault-propagation folds attain their near-final width during the early stages of deformation, while fold amplitude increases gradually at the same rate as increasing fault throw (e.g. Figs. 7 – 12). This is similar to physical models (e.g. Figs. 6 – 7 in Withjack et al., 1990; Figs. 6 – 8 in Miller and Mitra, 2011) and mechanical models (e.g. Fig. 7 in Finch et al., 2004; Fig. 5 in Patton, 2004; Fig. 2 in Hardy, 2011; Fig. 2 in Hardy, 2013; Fig. 3 in Smart and Ferrill, 2018). Likewise, seismic reflection studies (e.g. Fig. 4A in Corfield and Sharp, 2000; figures 4 and 6 in Corfield et al., 2001) indicate fault-propagation folds in nature also attain their near-final width early during extension, although typically poor imaging at substantial burial depths makes it difficult to constrain fold growth spatially and temporally in high-resolution. Furthermore, the forward models presented here provide a framework whereby natural structures and their associated growth strata may be compared to, and permit the relative importance of these parameters to be ranked.

Our analysis suggests that the P/S ratio is arguably, the most important control on the occurrence, geometry and evolution of a fault-propagation fold (Fig. 6C): the lower the P/S, the longer a point will reside in the trishear zone, and the greater opportunity the rock will have to deform (Williams and Chapman, 1983; Allmendinger et al., 2004; Pei et al., 2014). Regardless of other parameters, if the P/S ratio is very high, there is little time for the strata to become folded before the upper fault tip propagates through the succession and folding ceases. Therefore, P/S likely controls the occurrence of fault-propagation folds, or at least the propagation rate is the principal control (Hardy and Allmendinger, 2011). This is because the fault tip does not have to propagate into the cover even if the displacement rate is high (e.g. P/S ~ 0 for the forced folds in the Rhine Graben; Ford et al., 2007). In contrast, if the displacement rate is low, but the propagation rate is very high, the cover is breached rapidly and no folding occurs.

If there is sufficient time for the strata to become folded, the shape, size and evolution of the fault-propagation fold is increasingly influenced by the other parameters. Concentration factor, trishear symmetry, trishear angle and cover thickness may, in their extremes, inhibit the occurrence of fault-propagation folds, although this is still dependent on the P/S ratio. The fault dip has only a minor control on fold occurrence, as regardless of fault dip, a fault-propagation fold may form. In summary, we can rank the relative importance of the trishear parameters in terms of whether a fold develops at all, and whether they control subsequent fold shape: (1)

P/S; (2) concentration factor, (3) trishear symmetry, (4) trishear angle, (5) cover thickness (i.e. burial depth), and (6) fault dip.

What is the mechanical significance of the trishear parameters in nature?

Although trishear adequately describes the first-order geometry of growing fault-propagation folds, the mechanical significance of these trishear parameters are poorly understood. Here, we discuss the possible geological significance of each of the trishear parameters in turn, drawing on our forward modelling results and observations from natural examples (cf. Fig. 6).

The cover thickness reflects the burial depth at which the normal fault may nucleate (Fig. 15A – A'). Fault-propagation folds associated with very small cover thicknesses may form above near-surface faults (e.g. Reykjanes Peninsula, Iceland - Grant and Kattenhorn, 2004; Kilauea, Hawaii - Martel and Langley, 2006; Modoc Plateau, US - White and Crider, 2006; Blakeslee and Kattenhorn, 2013), whereas large cover thicknesses may be associated with thick-skinned rift systems (e.g. Halten Terrace, Norway - Corfield and Sharp, 2000; Coleman et al., 2017; Gulf of Suez, Egypt - Khalil and McClay, 2002; Farsund Basin, Norway - Phillips et al., 2018). Normal faults in the crust typically vary between 50° and 90° (Walsh and Watterson, 1988), and may be controlled by the depth in the crust at which the fault nucleates (Hardy and Ford, 1997), the dip of a pre-existing and subsequently reactivated structural weaknesses (Khalil and McClay, 2002; Pei et al., 2014), or lithological and rheological changes in the faulted host rock (Welch et al., 2009). For example, a shallowly-dipping shear zone formed during earlier contraction may be reactivated during later extension (cf. Khalil and McClay, 2002; Phillips et al., 2016) , and as such, newly formed faults may exploit the pre-existing weakness and inherit a shallow dip (Fig. 15B). In contrast, near-surface, sub-vertical fissures may be reactivated as steep-dipping normal faults during later extension (Fig. 15B'; e.g. Kaven and Martel, 2007; Trippanera et al., 2015; Bubeck et al., 2018).

Prior studies have speculated that the P/S ratio and the trishear angle may be related to the strength of the cover (e.g. lithology and mechanical heterogeneity; Hardy and Ford, 1997; Allmendinger, 1998; Hardy and McClay, 1999). This may explain why fold widths are greater and deformation is more distributed for weaker vs. stronger units, and multi-layer vs single-layers (Withjack et al., 1990; Patton et al., 1998; Finch et al., 2004). For example, salt or shale within a rheologically heterogeneous succession may inhibit fault-propagation (Fig. 15C; Couples et al., 1998; Roche et al., 2012, 2013), whereas homogeneous, rheologically strong and predominantly brittle cover comprised of, for example, igneous rock, or well-lithified carbonate or sandstone, may promote high propagation-to-slip ratios (Fig. 15C'; cf. Hardy and Finch, 2007; Welch et al., 2009; Pei et al., 2014). In addition, multi-layered ductile cover may cause widening of the trishear zone, promoting distributed deformation either by layer-parallel slip (cf. Withjack et al., 1990; Sharp et al., 2000a; Khalil and McClay, 2002; Welch et al., 2009) or tectonic thinning (cf. Brown, 1988; e.g. Finch et al., 2004; Egholm et al., 2007), (Fig. 15D). Conneally et al. (2017) suggest that the extent of the trishear zone could also be related to strain hardening, where, after a given amount of faulting and folding, the area over which future strain can occur narrows. Such strain deformation near the fault tip may also lead to higher P/S ratios. Furthermore, P/S ratio and trishear angle may be intimately related; as the trishear angle narrows, deformation is localised above the propagating fault tip, the fault tip may propagate more rapidly, and the folded cover may thus be breached earlier (cf. Figs. 9 – 10).

In a similar way to the P/S ratio and trishear angle, the concentration factor also controls the distribution of deformation in the vicinity of the fault tip (Fig. 11; 14). It might therefore be expected that the concentration factor may too reflect changes in the mechanical properties of the rock. High non-linear concentration factors, which are associated with little to no folding, may be related to brittle, mechanically homogeneous cover. In contrast, low non-linear concentration factors, which lead to multiple fold hinges (A_1 – A_3 in Fig. 11; A – A' in Fig. 14), may be associated with secondary faults that develop above and which may splay-off from, the underlying propagating fault tip. If secondary faults develop above the upper fault tip (e.g. Fig. 6 in Withjack et al., 1990; Fig. 7 and 17B in Sharp et al., 2000a; Fig. 10 in Allmendinger et al., 2004; Fig. 6 in Ferrill et al., 2011), it is possible that small-scale, 'parasitic' fault-propagation folds could form within the larger fault-propagation fold (Fig. 15E). Eventually, as the secondary faults are rotated in the footwall of and ultimately breached by later secondary faults (e.g. Withjack et al., 1990; Jackson et al., 2006), additional minor fold hinges may develop, changing the overall shape of the fold.

The final parameter that controls where and how deformation is distributed in the trishear model is trishear symmetry. Where trishear models have been used to replicate examples in nature and physical models, the trishear zone has rarely been symmetrical (Table 1 and references therein), but has not been explicitly linked to geological features in natural examples such as across-fault mechanical heterogeneity, pre-existing weaknesses or fault geometry (Fig. 15F – F'). If there was a mechanical difference between the footwall and hangingwall of the deforming host rock, it might be possible for the distribution of deformation to be asymmetric either side of the fault (Fig. 16). If a detachment horizon, such as salt, is present only in the hangingwall (e.g. Figs. 5 and 10 in Lewis et al., 2013; Fig. 16A), the extent of deformation may also be different either side of the fault. Alternatively, if the fault changes dip as it propagates upwards, the trishear angle and the degree of asymmetry may also change (e.g. Fig. 13A in Jin and Groshong, 2006). As discussed earlier, changes in fault dip may be due to lithology, strain hardening, burial depth or pre-existing weaknesses (cf. Fig. 15B).

An intra-cover detachment controls whether prekinematic cover is welded to the rigid basement, as is assumed in trishear models. During trishear, the cover is thinned or thickened to preserve cross-sectional area (Erslev, 1991; Hardy and Ford, 1997), although Stearns (1978) noted that, when the cover is not welded to the basement, it remains isopachous, whereas cover that is welded to the basement is thinned and stretched (e.g. Fig. 3 in Mitra, 1993). The degree of cover-basement welding also dictates the velocity distributions (ν_x and ν_y in Fig. 3) and thus, whether or not the sedimentary cover moves in the direction of faulting (Johnson and Johnson, 2002). Regardless of its mechanical heterogeneity, if the cover is welded to the basement, the cover moves in the direction of fault slip. If the cover is completely detached and is free to slip along the basement-cover contact, the cover moves vertically. If the cover is partially detached, the cover moves obliquely with respect to the fault (Johnson and Johnson, 2002). Trishear in contrast to mechanical models, thus only suitably describes cover that is welded to the basement (Zehnder and Allmendinger, 2000; Johnson and Johnson, 2002). Furthermore, if a detachment is present, such as thick salt and/or shale (e.g. Withjack and Callaway, 2000; Ford et al., 2007; Jackson and Lewis, 2016; Coleman et al., 2017; cf. Figs. 15C, 16A), this may permit the cover to slip relative to the basement, so that a trishear model may be invalid (Johnson and Johnson, 2002). Where there is an abrupt transition between faulting below and folding above a propagating fault tip due to the presence of an intra-cover detachment (cf. "forced folds" after Withjack and Callaway, 2000), in which case layer-parallel slip is likely, trishear may not be a valid kinematic model for understanding or reconstructing the growth of extensional fault-propagation folds.

What are the limitations of trishear?

Although kinematic models such as trishear reproduce the overall strain and geometry of fault-propagation folds in homogeneous sequences (Hardy and McClay, 1999; Cardozo et al., 2003; Cardozo et al., 2011), the simplicity of the velocity field is likely inadequate to capture the processes associated with mechanical heterogeneity (e.g. flexural slip, rheological heterogeneity, fluid pressure, compaction), or deformation associated with geometrically complex, non-planar faults (e.g. Fig. 5 in Johnson and Johnson, 2002). Trishear also assumes that deformation is geological instantaneous and strictly in-plane (Allmendinger, 1998); in reality, folding and faulting does not occur across the entirety of the fold instantaneously (Hardy, 2011), may vary along-strike (Sharp et al., 2000b; Conneally et al., 2017) and deformation may be oblique (Grant and Kattenhorn, 2004). This may affect how deformation is distributed in the vicinity of the propagating fault tip. Likewise, trishear models assume that there is a distinct mechanical contrast between the basement and the cover (e.g. Hardy and Ford, 1997), but this too is an oversimplification and may affect how strain is distributed in the vicinity of the fault. Furthermore, trishear models may not be appropriate for some scenarios. One such example, is for forced folds trishear models may not be appropriate for forced folds where high-resolution growth strata demonstrate the along-strike flow of ductile material within the detachment (e.g. Richardson et al., 2005). In addition and as noted by Ford et al. (2007), trishear models may only predict the geometry of a single fold at any one point in time. This has implications for structural restoration in ancient extensional basins, in which multiple folds may have grown at similar times and in the vicinity of one-another. Salt-rich basins containing large amounts of extension-related growth folding (e.g. Jackson and Lewis, 2016; Coleman et al., 2017) may again not be appropriate for trishear models. Ductile lithologies also may locally affect the velocity distribution in and around the trishear zone, and thus, it is perhaps unrealistic, especially for small fault displacements and low strain rates, where the hangingwall may deform in a ductile rather than brittle manner (e.g. Fig. 7 vs. 8 in Withjack and Callaway, 2000). Natural examples of fault-propagation folds are undoubtedly compacted as they are buried; however, post-formation processes like compaction are not normally incorporated explicitly into the trishear model (e.g. Khalil and McClay, 2002). Differential compaction may increase the amplitude of the fold and the dip of the fold limbs, but decrease the FSF for a given fault throw. Although trishear models without compaction closely resemble the geometry of fault-propagation folds in nature (cf. Table 1), the best-fit occurs when compaction is explicitly included (see Jin et al., 2009 for a discussion of compaction in trishear models).

By forward modelling fold geometry, the controlling trishear parameters can be determined (Allmendinger, 1998; Cardozo et al., 2003; Cardozo et al., 2011; Hardy and Allmendinger, 2011), and when used in conjunction with high-resolution growth strata, the evolution of the fold can be reconstructed through time and the geometric misfit between the model and natural example minimised. However, given the array of fold shapes that can be produced using the model parameters, a single solution often does not exist (e.g. Cardozo et al., 2011). Instead, a range of trishear parameters may be permissible, making it difficult to explicitly relate geological factors to particular trishear parameters. For example, uncertainty in the location of the fault tip will generate a wide range of acceptable models (Ford et al., 2007), with significant implications for other trishear parameters. To truly understand how folds grow and the controlling parameters on geometry and size, kinematic models need to be quantitatively compared with natural examples, and physical (e.g. Withjack et al., 1990) or mechanical models (e.g. Finch et al., 2004). We tackle this in Chapter 5. Further inverse modelling (Allmendinger, 1998; Cardozo et al., 2011) is also required to explore a realistic parameter space for natural examples.

Conclusions

By varying parameters in a kinematic trishear model, we predict the geometry and size of extensional fault-propagation fold geometry. We suggest that fold amplitude is dependent primarily on fault throw, while width, which more strongly controls the FSF (as fold width typically has a greater range than amplitude) and fold limb dip through time is very dependent on cover thickness, propagation-to-slip ratio, trishear angle, concentration factor and shear symmetry. Our analysis suggests that the propagation-to-slip ratio is the dominant control on fold growth, and only when the propagation-to-slip ratio is relatively low, may the other trishear parameters exert a control on the fold shape and development.

Trishear models predict that fold width is established relatively early and rapidly while fold amplitude is accrued gradually during extension. However, further comparisons need to be undertaken in order to investigate whether the same is true for physical models and in nature (see Chapter 5). Especially given that kinematic models do not consider complexities such as mechanical and rheological heterogeneity.

We do not pretend to understand what these trishear parameters correlate to in nature, but we propose a geological reason for each which reflect rheological heterogeneity, pre-existing weaknesses, secondary deformation, the depth of fault nucleation. This highlights possible factors that may be investigated in future work.

Finally, our forward models show that the architecture of synkinematic strata, if deposited at the same or a greater rate than the fold growth rate, are highly sensitive to model parameters. Model parameters that promote wide folds dramatically affect the lateral width over which synkinematic strata thin. In contrast, as the fold amplitude is related to fault throw, the ratio between the hangingwall and footwall thickness is largely similar irrespective of the model parameters. With that said, we show that parameters that prolong the folding duration are characterised by fold-related synkinematic wedges, while rapid fold breaching, are characterised by abrupt, step-like synkinematic strata that thicken towards the surface-breached fault, for much of the extension duration.

References

Allmendinger, R. W., 1998, Inverse and forward numerical modeling of trishear fault-propagation folds: Tectonics, v. 17, no. 4, p. 640-656.

Allmendinger, R. W., Zapata, T., Manceda, R., and Dzelalija, F., 2004, Trishear Kinematic Modeling of Structures, with Examples from the Neuqun Basin, Argentina, *in* McClay, K., ed., Thrust tectonics and hydrocarbon systems, Volume 82, AAPG Memoir, p. 1-17.

Barnett, J. A., Mortimer, J., Rippon, J. H., Walsh, J. J., and Watterson, J., 1987, Displacement geometry in the volume containing a single normal fault: AAPG Bulletin, v. 71, no. 8, p. 925-937.

Blakeslee, M. W., and Kattenhorn, S. A., 2013, Revised earthquake hazard of the Hat Creek fault, northern California: A case example of a normal fault dissecting variable-age basaltic lavas: Geosphere, v. 9, no. 5, p. 1397-1409.

Botter, C., Cardozo, N., Hardy, S., Lecomte, I., and Escalona, A., 2014, From mechanical modeling to seismic imaging of faults: A synthetic workflow to study the impact of faults on seismic: Marine and Petroleum Geology, v. 57, p. 187-207.

Brown, W. G., 1988, Deformational style of Laramide uplifts in the Wyoming foreland: Interaction of the Rocky Mountain foreland and the Cordilleran thrust belt: Geological Society of America Memoir, v. 171, p. 1-25.

Bubeck, A., Walker, R. J., Imber, J., and MacLeod, C. J., 2018, Normal fault growth in layered basaltic rocks: The role of strain rate in fault evolution: Journal of Structural Geology, v. 115, p. 103-120.

Cardozo, N., Bhalla, K., Zehnder, A. T., and Allmendinger, R. W., 2003, Mechanical models of fault propagation folds and comparison to the trishear kinematic model: Journal of Structural Geology, v. 25, no. 1, p. 1-18.

Cardozo, N., Jackson, C. A.-L., and Whipp, P. S., 2011, Determining the uniqueness of best-fit trishear models: Journal of Structural Geology, v. 33, no. 6, p. 1063-1078.

Coleman, A. J., Jackson, C. A.-L., and Duffy, O. B., 2017, Balancing sub- and supra-salt strain in salt-influenced rifts: Implications for extension estimates: Journal of Structural Geology, v. 102, p. 208-225.

Conneally, J., Childs, C., and Nicol, A., 2017, Monocline formation during growth of segmented faults in the Taranaki Basin, offshore New Zealand: Tectonophysics, v. 721, p. 310-321.

Corfield, S., and Sharp, I., 2000, Structural style and stratigraphic architecture of fault propagation folding in extensional settings: a seismic example from the Smørbukk area, Halten Terrace, Mid-Norway: Basin Research, v. 12, no. 3-4, p. 329-341.

Corfield, S., Sharp, I., Häger, K.-O., Dreyer, T., and Underhill, J., 2001, An integrated study of the garn and melke formations (middle to upper jurassic) of the smorbukk area, halten terrace, mid-norway, *in* Ole, J. M., and Tom, D., eds., Norwegian Petroleum Society Special Publications, Volume Volume 10, Elsevier, p. 199-210.

Couples, G. D., Lewis, H., and Tanner, P. G., 1998, Strain partitioning during flexural-slip folding: Geological Society, London, Special Publications, v. 127, no. 1, p. 149-165.

Cowie, P. A., 1998, A healing–reloading feedback control on the growth rate of seismogenic faults: Journal of Structural Geology, v. 20, no. 8, p. 1075-1087.

Cowie, P. A., Underhill, J. R., Behn, M. D., Lin, J., and Gill, C. E., 2005, Spatio-temporal evolution of strain accumulation derived from multi-scale observations of Late Jurassic rifting in the northern North Sea: A critical test of models for lithospheric extension: Earth and Planetary Science Letters, v. 234, no. 3–4, p. 401-419.

Crider, J. G., Cooke, M. L., Willemse, E. J. M., and Arrowsmith, J. R., 1996, Linear-elastic crack models of jointing and faulting, *in* De Paor, D. G., ed., Computer Methods in the Geosciences, Volume 15, Pergamon, p. 359-388.

d'Alessio, M. A., and Martel, S. J., 2004, Fault terminations and barriers to fault growth: Journal of structural geology, v. 26, no. 10, p. 1885-1896.

Egholm, D. L., Sandiford, M., Clausen, O. R., and Nielsen, S. B., 2007, A new strategy for discrete element numerical models: 2. Sandbox applications: Journal of Geophysical Research: Solid Earth, v. 112, no. 1-12.

Erslev, E. A., 1991, Trishear fault-propagation folding: Geology, v. 19, no. 6, p. 617.

Ferrill, D. A., Morris, A. P., McGinnis, R. N., Smart, K. J., and Ward, W. C., 2011, Fault zone deformation and displacement partitioning in mechanically layered carbonates: The Hidden Valley fault, central Texas: AAPG Bulletin, v. 95, no. 8, p. 1383-1397.

Finch, E., Hardy, S., and Gawthorpe, R., 2004, Discrete-element modelling of extensional fault-propagation folding above rigid basement fault blocks: Basin Research, v. 16, no. 4, p. 467-488.

Ford, M., Le Carlier de Veslud, C., and Bourgeois, O., 2007, Kinematic and geometric analysis of fault-related folds in a rift setting: The Dannemarie basin, Upper Rhine Graben, France: Journal of Structural Geology, v. 29, no. 11, p. 1811-1830.

Gawthorpe, R. L., Sharp, I., Underhill, J. R., and Gupta, S., 1997, Linked sequence stratigraphic and structural evolution of propagating normal faults: Geology, v. 25, no. 9, p. 795.

Gawthorpe, R. L., and Leeder, M. R., 2000, Tectono-sedimentary evolution of active extensional basins: Basin Research, v. 12, no. 3-4, p. 195-218.

Gawthorpe, R. L., and Hardy, S., 2002, Extensional fault-propagation folding and base-level change as controls on growth-strata geometries: Sedimentary Geology, v. 146, no. 1, p. 47-56.

Grant, J. V., and Kattenhorn, S. A., 2004, Evolution of vertical faults at an extensional plate boundary, southwest Iceland: Journal of Structural Geology, v. 26, no. 3, p. 537-557.

Gupta, S., Underhill, J., Sharp, I., and Gawthorpe, R., 1999, Role of fault interactions in controlling synrift sediment dispersal patterns: Miocene, Abu Alaqa Group, Suez Rift, Sinai, Egypt: Basin Research, v. 11, no. 2, p. 167-189.

Hardy, S., and Ford, M., 1997, Numerical modeling of trishear fault propagation folding: Tectonics, v. 16, no. 5, p. 841-85

Hardy, S., and McClay, K., 1999, Kinematic modelling of extensional fault-propagation folding: Journal of Structural Geology, v. 21, no. 7, p. 695-702.

Hardy, S., Poblet, J., McClay, K., and Waltham, D., 1999, Mathematical modelling of growth strata associated with fault-related fold structures: Geological Society, London, Special Publications, v. 99, no. 1, p. 265-282.

Hardy, S., and Finch, E., 2006, Discrete element modelling of the influence of cover strength on basement-involved fault-propagation folding: Tectonophysics, v. 415, no. 1-4, p. 225-238.

Hardy, S., and Finch, E., 2007, Mechanical stratigraphy and the transition from trishear to kink-band fault-propagation fold forms above blind basement thrust faults: A discrete-element study: Marine and Petroleum Geology, v. 24, no. 2, p. 75-90.

Hardy, S., 2011, Cover deformation above steep, basement normal faults: Insights from 2D discrete element modeling: Marine and Petroleum Geology, v. 28, no. 5, p. 966-972.

Hardy, S., and Allmendinger, R. W., 2011, Trishear: A review of kinematics, mechanics, and applications, *in* McClay, K., ed., Thrust fault-related folding, AAPG Memoir 94, AAPG, p. 95-119.

Hardy, S., 2013, Propagation of blind normal faults to the surface in basaltic sequences: Insights from 2D discrete element modelling: Marine and Petroleum Geology, v. 48, no. 0, p. 149-159.

Horsfield, W., 1977, An experimental approach to basement-controlled faulting: Geologie en Mijnbouw, v. 56, no. 4, p. 363-370.

Hossack, J. R., 1979, The use of balanced cross-sections in the calculation of orogenic contraction: A review: Journal of the Geological Society, v. 136, no. 6, p. 705-711.

Jackson, C. A.-L., Gawthorpe, R. L., and Sharp, I. R., 2006, Style and sequence of deformation during extensional fault-propagation folding: examples from the Hammam Faraun and El-Qaa fault blocks, Suez Rift, Egypt: Journal of Structural Geology, v. 28, no. 3, p. 519-535.

Jackson, C. A.-L., and Lewis, M. M., 2013, Physiography of the NE margin of the Permian Salt Basin: new insights from 3D seismic reflection data: Journal of the Geological Society, v. 170, no. 6, p. 857-860.

Jackson, C. A.-L., Corfield, S., and Dreyer, T., 2017, Temporal evolution of extensional fault-propagation folds: EarthArXiv.

Jackson, C. A. L., and Lewis, M. M., 2016, Structural style and evolution of a salt-influenced rift basin margin; the impact of variations in salt composition and the role of polyphase extension: Basin Research, v. 28, no. 1, p. 81-102.

Jin, G., and Groshong, R. H., 2006, Trishear kinematic modeling of extensional fault-propagation folding: Journal of Structural Geology, v. 28, no. 1, p. 170-183.

Jin, G., Groshong, R. H., and Pashin, J. C., 2009, Growth trishear model and its application to the Gilbertown graben system, southwest Alabama: Journal of Structural Geology, v. 31, no. 9, p. 926-940.

Johnson, K. M., and Johnson, A. M., 2002, Mechanical models of trishear-like folds: Journal of Structural Geology, v. 24, no. 2, p. 277-287.

Kaven, J. O., and Martel, S. J., 2007, Growth of surface-breaching normal faults as a three-dimensional fracturing process: Journal of Structural Geology, v. 29, no. 9, p. 1463-1476.

Khalil, S., and McClay, K., 2002, Extensional fault-related folding, northwestern Red Sea, Egypt: Journal of Structural Geology, v. 24, no. 4, p. 743-762.

Khalil, S. M., and McClay, K. R., 2016, 3D geometry and kinematic evolution of extensional fault-related folds, NW Red Sea, Egypt: Geological Society, London, Special Publications, v. 439, p. 1-11.

Lewis, M. M., Jackson, C. A.-L., and Gawthorpe, R. L., 2013, Salt-influenced normal fault growth and forced folding: The Stavanger Fault System, North Sea: Journal of Structural Geology, v. 54, p. 156-173.

Lewis, M. M., Jackson, C. A.-L., Gawthorpe, R. L., and Whipp, P. S., 2015, Early synrift reservoir development on the flanks of extensional forced folds: A seismic-scale outcrop analog from the Hadahid Fault System, Suez Rift, Egypt: AAPG Bulletin, no. 20,150,119.

Lingrey, S., and Vidal-Royo, O., 2015, Evaluating the quality of bed length and area balance in 2D structural restorations: Interpretation, v. 3, no. 4, p. SAA133-SAA160.

Marsh, N., Imber, J., Holdsworth, R., Brockbank, P., and Ringrose, P., 2010, The structural evolution of the Halten Terrace, offshore Mid-Norway: extensional fault growth and strain localisation in a multi-layer brittle–ductile system: Basin Research, v. 22, no. 2, p. 195-21

Martel, S. J., and Langley, J. S., 2006, Propagation of normal faults to the surface in basalt, Koae fault system, Hawaii: Journal of Structural Geology, v. 28, no. 12, p. 2123-2143.

Meyer, V., Nicol, A., Childs, C., Walsh, J., and Watterson, J., 2002, Progressive localisation of strain during the evolution of a normal fault population: Journal of Structural Geology, v. 24, no. 8, p. 1215-1231.

Miller, J. F., and Mitra, S., 2011, Deformation and secondary faulting associated with basement-involved compressional and extensional structures: AAPG bulletin, v. 95, no. 4, p. 675-689.

Mitra, S., 1993, Geometry and kinematic evolution of inversion structures: AAPG Bulletin, v. 77, no. 7, p. 1159-1191.

Mueller, K., 2017, Variation in slip rates on active faults: Natural growth or stress transients?: Geology, v. 45, no. 3, p. 287-288.

Nicol, A., Walsh, J., Watterson, J., and Underhill, J., 1997, Displacement rates of normal faults: Nature, v. 390, no. 6656, p. 157.

Pascoe, R., Hooper, R., Storhaug, K., and Harper, H., 1999, Evolution of extensional styles at the southern termination of the Nordland Ridge, Mid-Norway: a response to variations in coupling above Triassic salt: Petroleum Geology Conference Series, v. 5, p. 83-90.

Patton, T. L., Logan, J. M., and Friedman, M., 1998, Experimentally generated normal faults in single-layer and multilayer limestone specimens at confining pressure: Tectonophysics, v. 295, no. 1, p. 53-77.

Patton, T. L., 2004, Numerical models of growth-sediment development above an active monocline: Basin Research, v. 16, p. 25-39.

Pei, Y., Paton, D. A., and Knipe, R. J., 2014, Defining a 3-dimensional trishear parameter space to understand the temporal evolution of fault propagation folds: Journal of structural Geology, v. 66, p. 284-297.

Phillips, T. B., Jackson, C. A.-L., Bell, R. E., Duffy, O. B., and Fossen, H., 2016, Reactivation of intrabasement structures during rifting: A case study from offshore southern Norway: Journal of Structural Geology, v. 91, p. 54-73.

Phillips, T. B., Jackson, C. A.-L., Bell, R. E., and Duffy, O. B., 2018, Oblique reactivation of lithosphere-scale lineaments controls rift physiography–the upper-crustal expression of the Sorgenfrei–Tornquist Zone, offshore southern Norway: Solid Earth, v. 9, no. 2, p. 403.

Pollard, D. D., and Segall, P., 1987, Theoretical displacements and stresses near fractures in rock: with applications to faults, joints, veins, dikes, and solution surfaces, *in* Atkinson, B. K., ed., Fracture Mechanics of Rock: London, Academic Press, p. 277-349.

Richardson, N. J., Underhill, J. R., and Lewis, G., 2005, The role of evaporite mobility in modifying subsidence patterns during normal fault growth and linkage, Halten Terrace, Mid-Norway: Basin Research, v. 17, no. 2, p. 203-223.

Roche, V., Homberg, C., and Rocher, M., 2012, Fault displacement profiles in multilayer systems: from fault restriction to fault propagation: Terra Nova, v. 24, no. 6, p. 499-50

Roche, V., Homberg, C., and Rocher, M., 2013, Fault nucleation, restriction, and aspect ratio in layered sections: quantification of the strength and stiffness roles using numerical modeling: Journal of Geophysical Research: Solid Earth, v. 118, no. 8, p. 4446-4460.

Rowan, M. G., and Kligfield, R., 1989, Cross section restoration and balancing as aid to seismic interpretation in extensional terranes: AAPG bulletin, v. 73, no. 8, p. 955-966.

Sharp, I., Gawthorpe, R., Armstrong, B., and Underhill, J., 2000a, Propagation history and passive rotation of mesoscale normal faults: implications for synrift stratigraphic development: Basin Research, v. 12, no. 3-4, p. 285-305.

Sharp, I. R., Gawthorpe, R. L., Underhill, J. R., and Gupta, S., 2000b, Fault-propagation folding in extensional settings: Examples of structural style and synrift sedimentary response from the Suez rift, Sinai, Egypt: Geological Society of America Bulletin, v. 112, no. 12, p. 1877-1899.

Smart, K. J., and Ferrill, D. A., 2018, Discrete element modeling of extensional fault-related monocline formation: Journal of Structural Geology, v. 115, p. 82-90.

Stearns, D. W., 1978, Faulting and forced folding in the Rocky Mountains foreland: Geological Society of America Memoirs, v. 151, p. 1-38.

Tavani, S., Balsamo, F., and Granado, P., 2018, Petroleum system in supra-salt strata of extensional forced-folds: A case-study from the Basque-Cantabrian basin (Spain): Marine and Petroleum Geology, v. 96, p. 315 - 330.

Trippanera, D., Acocella, V., Ruch, J., and Abebe, B., 2015, Fault and graben growth along active magmatic divergent plate boundaries in Iceland and Ethiopia: Tectonics, v. 34, no. 11, p. 2318-2348.

Tsuneishi, Y., 1978, Geological and Experimental Studies on Mechanism of Block Faulting.

Walsh, J. J., and Watterson, J., 1988, Dips of normal faults in British Coal Measures and other sedimentary sequences: Journal of the Geological Society, v. 145, no. 5, p. 859-873.

Waltham, D., and Hardy, S., 1995, The velocity description of deformation. paper 1: theory: Marine and Petroleum Geology, v. 12, no. 2, p. 153-163.

Welch, M. J., Knipe, R. J., Souque, C., and Davies, R. K., 2009, A Quadshear kinematic model for folding and clay smear development in fault zones: Tectonophysics, v. 471, no. 3, p. 186-202.

White, I. R., and Crider, J. G., 2006, Extensional fault-propagation folds: mechanical models and observations from the Modoc Plateau, northeastern California: Journal of Structural Geology, v. 28, no. 7, p. 1352-1370.

Wickham, J., and Moeckel, G., 1997, Restoration of structural cross-sections: Journal of Structural Geology, v. 19, no. 7, p. 975-986.

Williams, G., and Chapman, T., 1983, Strains developed in the hangingwalls of thrusts due to their slip/propagation rate: a dislocation model: Journal of Structural Geology, v. 5, no. 6, p. 563-571.

Withjack, M. O., Meisling, K. E., and Russell, L. R., 1989, Forced Folding and Basement-Detached Normal Faulting in the Haltenbanken Area, Offshore Norway: Chapter 37: North Sea and Barents Shelf, *in* Tankard, A. J., and Balkwill, H. R., eds., Extensional Tectonics and Stratigraphy of the North Atlantic Margins, AAPG Memoir 46, p. 567-575.

Withjack, M. O., Olson, J., and Peterson, E., 1990, Experimental models of extensional forced folds: AAPG Bulletin, v. 74, no. 7, p. 1038-105

Withjack, M. O., and Callaway, S., 2000, Active normal faulting beneath a salt layer: an experimental study of deformation patterns in the cover sequence: AAPG bulletin, v. 84, no. 5, p. 627-651.

Zehnder, A. T., and Allmendinger, R. W., 2000, Velocity field for the trishear model: Journal of Structural Geology, v. 22, no. 8, p. 1009-101

Zhao, H., Guo, Z., and Yu, X., 2017, Strain modelling of extensional fault-propagation folds based on an improved non-linear trishear model: A numerical simulation analysis: Journal of Structural Geology, v. 95, p. 60-76.

Figure captions

Figure 1. - Development of a fault-propagation fold above a 70° dipping normal fault, modified from Finch et al. (2004). The thickness of the prekinematic strata is 22 units, equivalent to ~ 5.5 km. Model width is 150 units, equivalent to ~ 37.5 km. Displacement is (A) 1.5 units, ~375 m; (B) 3.5 units, ~ 875 m; and (C) 7.5 units, ~ 1875 m. Layering is for visualisation only.

Figure 2. - Examples of fault-propagation folds in physical models (A - Withjack et al., 1990), numerical models (B - Allmendinger, 1998; Jackson et al., 2006), seismic reflection data (C, D – Lewis et al., 2015) and in the field (E, F – Lewis et al., 2015). Inset in F shows the context of the synkinematic strata in the field outcrop photograph (E) and interpretation (F) with respect to the Hadahid Monocline, Gulf of Suez, Egypt (Lewis et al., 2015).

Figure 3. - (A) The trishear velocity field. Velocities are uniform and parallel to the fault in the hangingwall and zero in the footwall. (B) The velocity distribution in the trishear zone is derived using Equations 1 – Modified after Hardy and Ford (1997), Allmendinger (1998), Zehnder and Allmendinger (2000), and Johnson and Johnson (2002).

Figure 4. - Trishear parameters and terminology. Terminology after Erslev (1991), Hardy and Ford (1997), Allmendinger (1998), and Zehnder and Allmendinger (2000).

Figure 5. - Schematic showing parameters and terminology for the description of synkinematic growth strata. The hangingwall-to-footwall thickness ratio (HW:FW) is the maximum vertical thickness of the synkinematic hangingwall strata divided by the footwall strata.

Figure 6. - Predictions of fold geometry and size, and synkinematic strata architecture derived from forward trishear models, corresponding to changes in (A) cover thickness, (B) fault dip, (C) propagation-to-slip ratio, (D) trishear angle, (E) concentration factor, (F) trishear symmetry. Left column – poorly-developed folds associated with typically shorter periods of folding which are breached relatively early during fold growth. Right column – well-developed folds associated with typically longer durations of folding which are breached relatively late during fold growth.

Figure 7. - Effect of cover thickness on fold geometry, size and synkinematic architecture with increasing fault throw. Plots for the fold amplitude, width, fold-shape-factor (FSF) and fold limb dip are also shown for thin (filled circles; black line) and thick (hollow circles; grey line) cover thicknesses. Panels A1 - A4 and B1 - B4 represent snapshots of the fold growth for a given fault throw. Fold breaching is shown on the plots where the line stops. Details of the forward models are described in Table 2.

Figure 8. - Effect of fault dip on fold geometry, size and synkinematic architecture with increasing fault throw. Plots for the fold amplitude, width, fold-shape-factor (FSF) and fold limb dip are also shown for shallow (hollow circles; grey line) and steep (filled circles; black line) fault dips. Panels A1 - A4 and B1 - B4 represent snapshots of the fold growth for a given fault throw. Fold breaching is shown on the plots where the line stops. Details of the forward models are described in Table 2.

Figure 9. - Effect of the propagation-to-slip (P/S) ratio on fold geometry, size and synkinematic architecture with increasing fault throw. Plots for the fold amplitude, width, fold-shape-factor (FSF) and fold limb dip are also shown for low (hollow circles; grey line) and high (filled circles; black line) P/S ratios. Panels A1 - A4 and B1 - B4 represent snapshots of the fold growth

for a given fault throw. Fold breaching is shown on the plots where the line stops. Details of the forward models are described in Table 2.

Figure 10. - Effect of the trishear angle on fold geometry, size and synkinematic architecture with increasing fault throw. Plots for the fold amplitude, width, fold-shape-factor (FSF) and fold limb dip are also shown for large (hollow circles; grey line) and small (filled circles; black line) trishear angles. Panels A1 - A4 and B1 - B4 represent snapshots of the fold growth for a given fault throw. Fold breaching is shown on the plots where the line stops. Details of the forward models are described in Table 2.

Figure 11. - Effect of the concentration factor on fold geometry, size and synkinematic architecture with increasing fault throw. Plots for the fold amplitude, width, fold-shape-factor (FSF) and fold limb dip are also shown for low, non-linear (hollow circles; grey line) and linear (filled circles; black line) concentration factors. Panels A1 - A4 and B1 - B4 represent snapshots of the fold growth for a given fault throw. Fold breaching is shown on the plots where the line stops. Details of the model is described in Table 2. White arrows indicate synkinematic onlap.

Figure 12. - Effect of trishear symmetry on fold geometry, size and synkinematic architecture with increasing fault throw. Panels A1 - A4 and B1 - B4 represent snapshots of the fold growth for a given fault throw. Plots for the fold amplitude, width, fold-shape-factor (FSF) and fold limb dip are also shown. As all of the asymmetrical folds were breached and had negligible amounts of folding, only the symmetrical trishear folds were plotted. Fold breaching is shown on the plots where the line stops. Details of the forward models are described in Table 2.

Figure 13. - Effect of the trishear parameters on the width of thinning (left) and hangingwall-to-footwall (HW:FW) thickness ratio (right) for synkinematic strata with increasing fault throw. Circles represent the snapshots of fold growth shown in Figs. 7 - 12. (A) - cover thickness, (B) – fault dip, (C) – propagation-to-slip ratio, (D) – trishear angle, (E) – concentration factor, and (F) trishear symmetry.

Figure 14. - Summary for how concentration factor (CF) may lead to complex synkinematic stacking patterns. (A – A') – very low, non-linear concentration factors ~ 0.5, (B – B') – linear, concentration factor ~ 1.0, and (C – C') – very high, non-linear concentration factor ~ 2. The fault-propagation fold geometry is shown (A – C). To highlight the width of thinning and

complex thinning pattern (yellow), the top of the prekinematic strata (white) and basement (hatched) has been flattened and restored. White arrows indicate onlap onto the fold.

Figure 15. - Possible causes of variations in trishear parameters due to geological factors. (A) – cover thickness, (B) – fault dip, (C) – propagation-to-slip ratio, (D) – trishear angle, (E) – concentration factor, and (F) – trishear symmetry.

Figure 16. - Possible causes of trishear asymmetry. (A) – Salt pinches out in the footwall allowing deformation to be focused into the hangingwall. (B) – Asymmetric damage zone due to early linkage and formation of a through-going fault may cause deformation to be focused preferentially into the hangingwall.

Table 1. - Trishear comparisons to published fault-propagation folds in physical and numerical models, and in natural examples. *Values not explicitly recorded by the original study, but measured by this work.

Table 2. - Specifications for the trishear forward models shown in Figs. 7 - 13. Only a single trishear parameter was tested in any particular run. The investigated parameter for a particular model run is shaded. The corresponding figures are also indicated.

Fig. 1

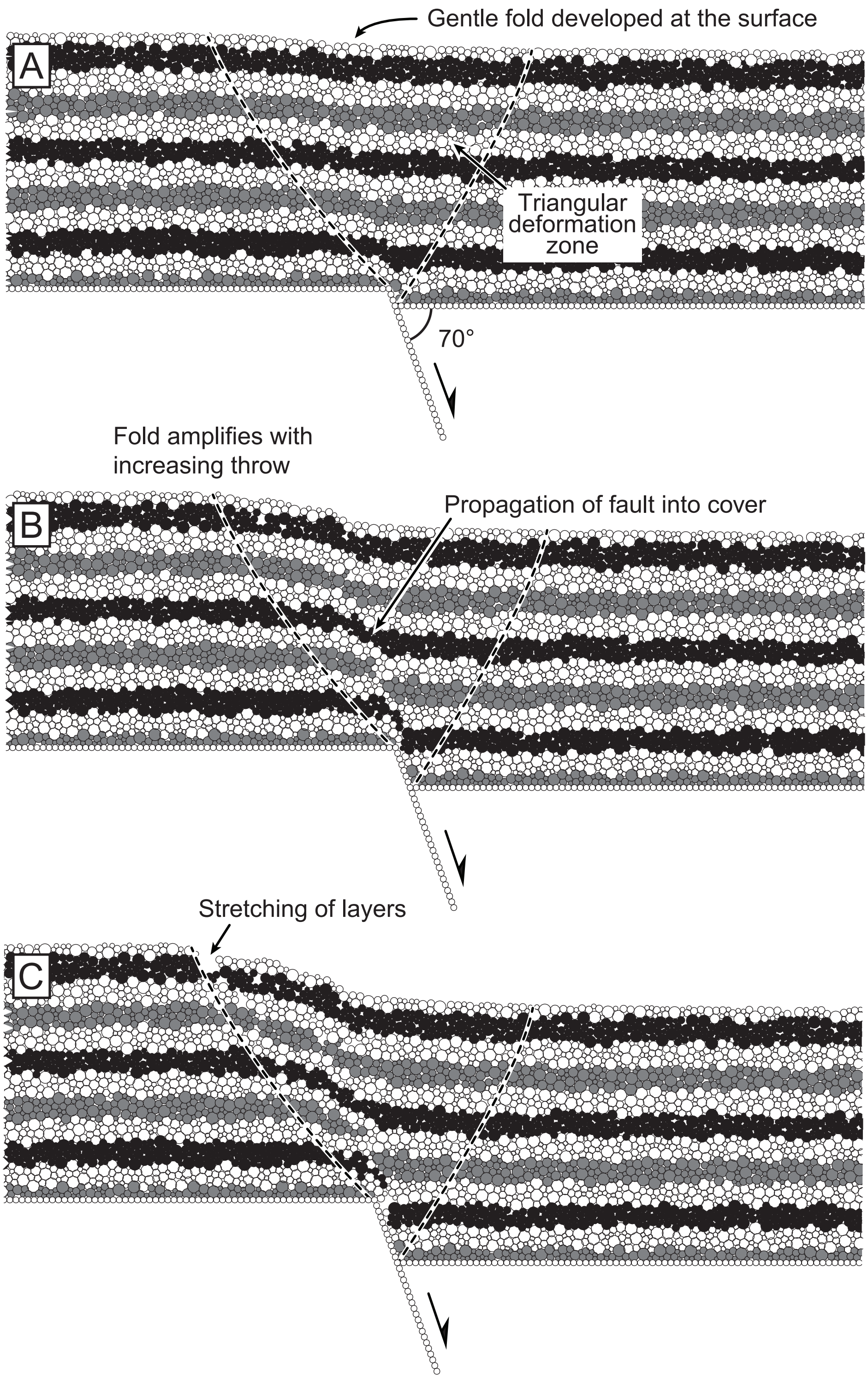
Gentle fold developed at the surface
A
Triangular deformation zone
70°
Fold amplifies with increasing throw
B
Propagation of fault into cover
Stretching of layers
C

Fig. 2

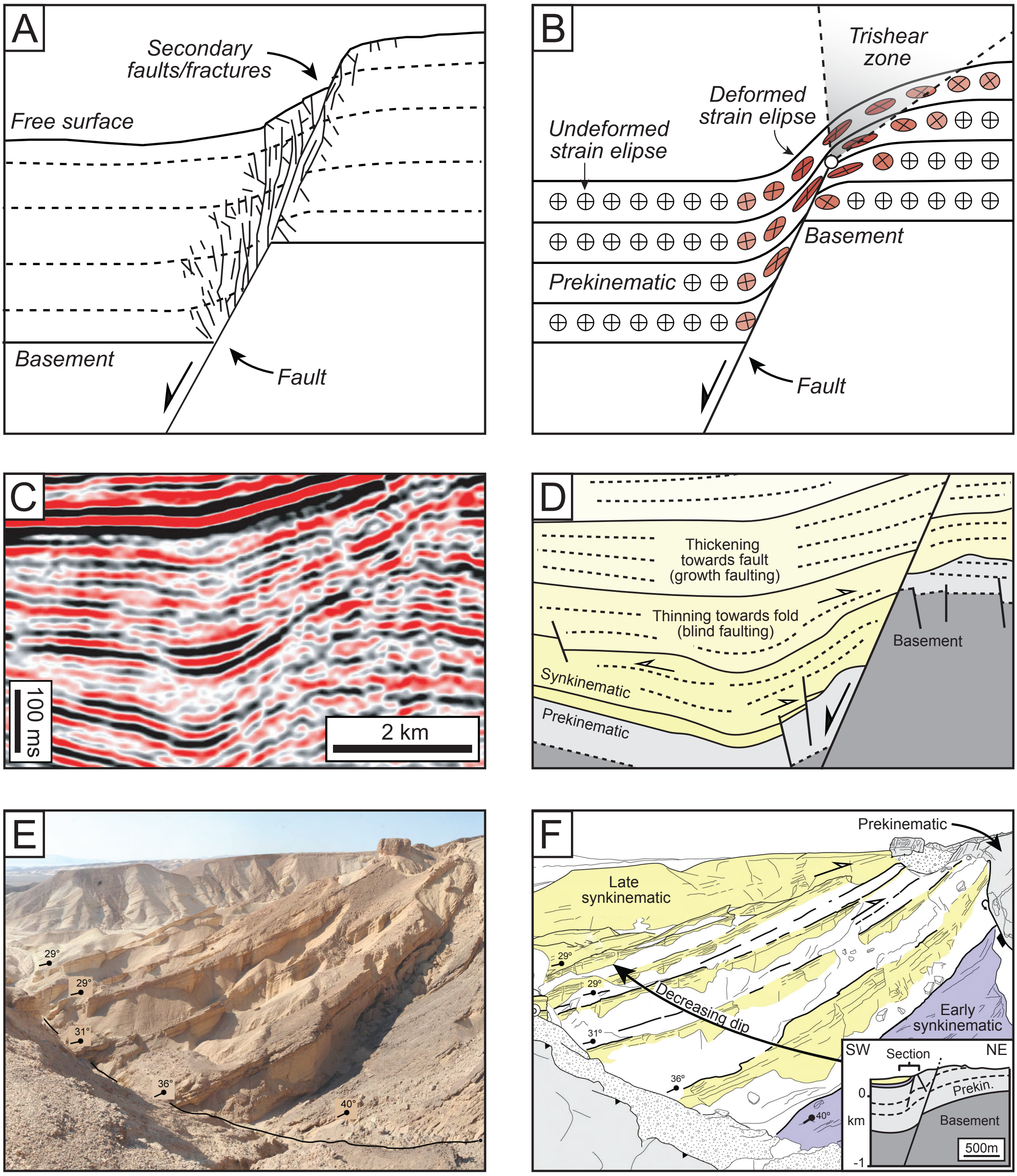

A
Secondary faults/fractures
Free surface
Basement
Fault
B
Trishear zone
Deformed strain elipse
Undeformed strain elipse
Basement
Prekinematic
Fault
C
100 ms
2 km
D
Thickening towards fault (growth faulting)
Thinning towards fold (blind faulting)
Synkinematic
Prekinematic
Basement
E
29°
29°
31°
36°
40°
F
Prekinematic
Late synkinematic
Decreasing dip
Early synkinematic
29°
29°
31°
36°
40°
SW
Section
NE
0
km
-1
Prekin.
Basement
500m

Fig. 3

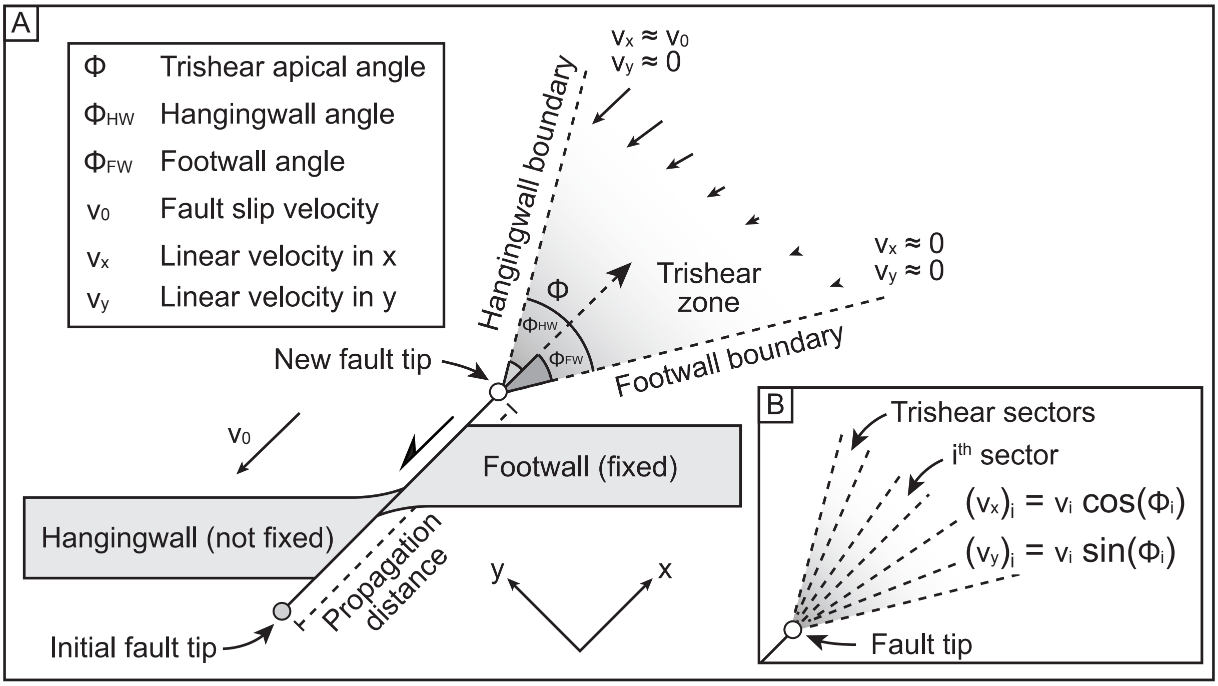
A
Φ Trishear apical angle
ΦHW Hangingwall angle
ΦFW Footwall angle
v0 Fault slip velocity
vx Linear velocity in x
vy Linear velocity in y
vx ≈ v0
vy ≈ 0
Hangingwall boundary
Φ
ΦHW
ΦFW
Trishear zone
vx ≈ 0
vy ≈ 0
Footwall boundary
New fault tip
v0
Footwall (fixed)
Hangingwall (not fixed)
Propagation distance
y
x
Initial fault tip
B
Trishear sectors
ith sector
(vx)i = vi cos(Φi)
(vy)i = vi sin(Φi)
Fault tip

Fig. 4

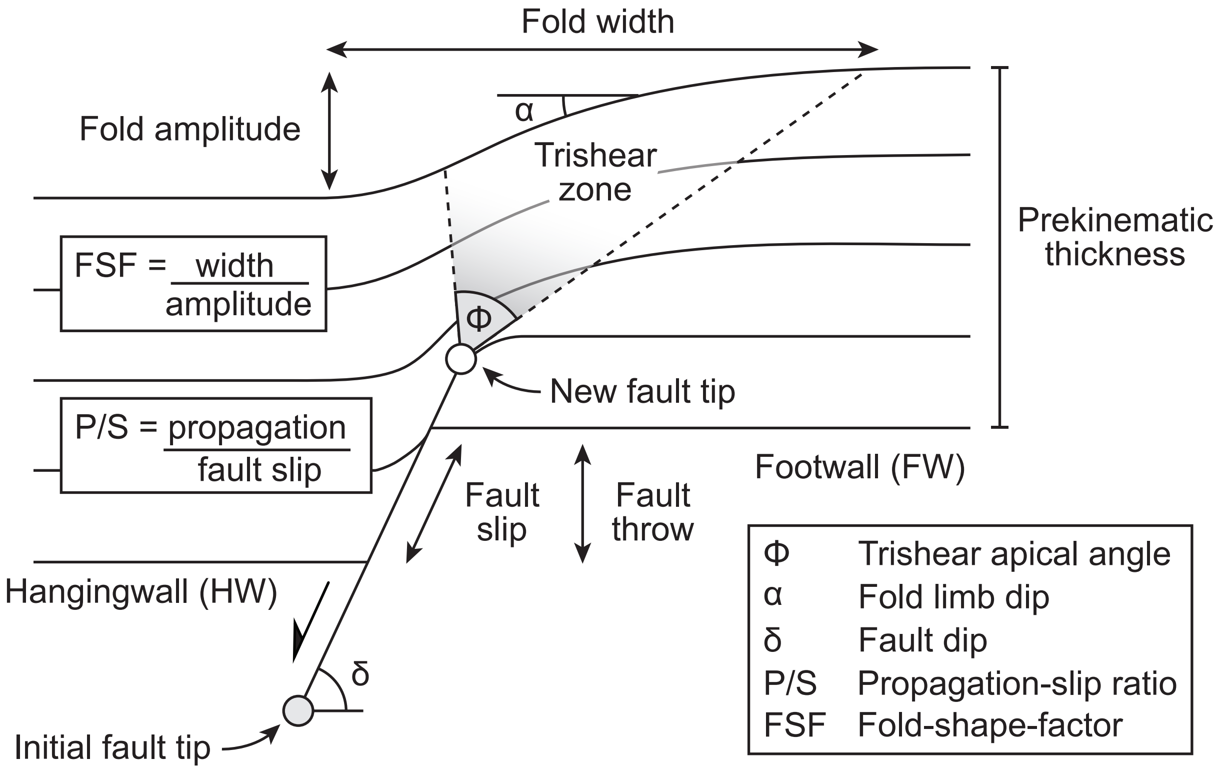
Fold width
Fold amplitude
α
Trishear
zone
Prekinematic
thickness
FSF = width / amplitude
Φ
New fault tip
P/S = propagation / fault slip
Footwall (FW)
Fault
slip
Fault
throw
Hangingwall (HW)
δ
Initial fault tip
Φ Trishear apical angle
α Fold limb dip
δ Fault dip
P/S Propagation-slip ratio
FSF Fold-shape-factor

Fig. 5

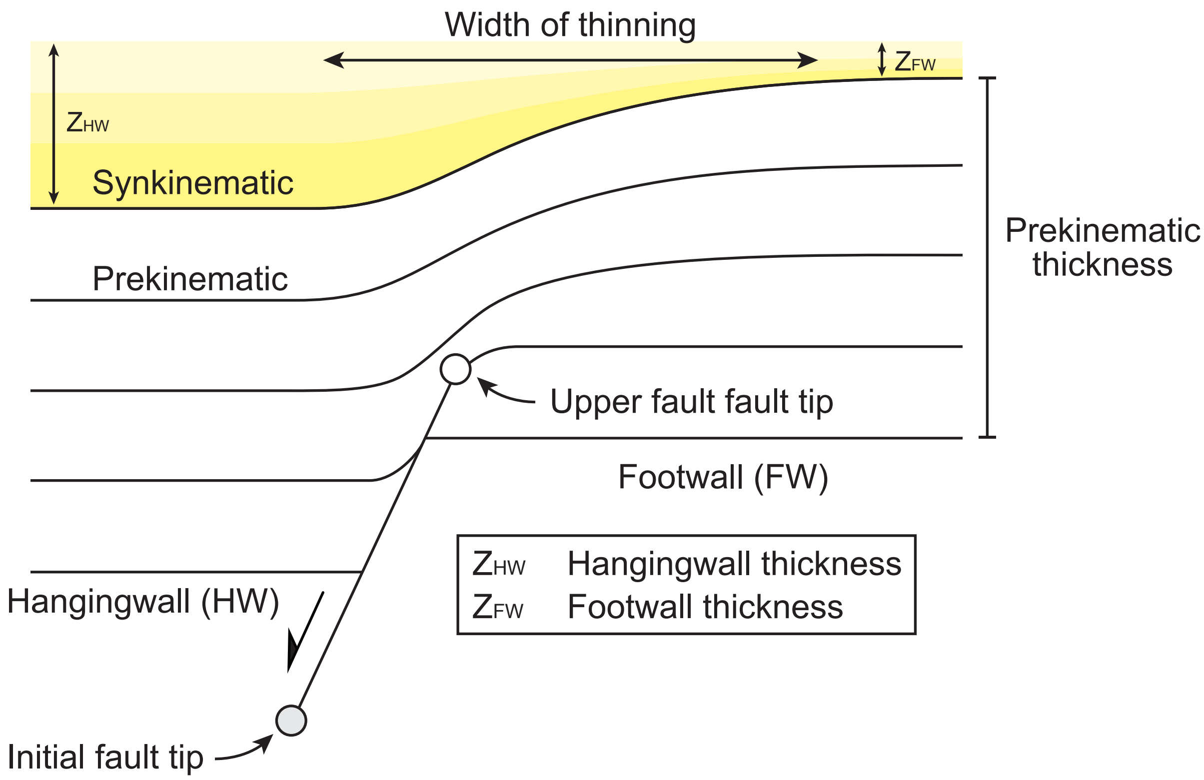

Width of thinning
Z_{FW}
Z_{HW}
Synkinematic
Prekinematic
Prekinematic thickness
Upper fault fault tip
Footwall (FW)
Z_{HW} Hangingwall thickness
Z_{FW} Footwall thickness
Hangingwall (HW)
Initial fault tip

Fig. 6

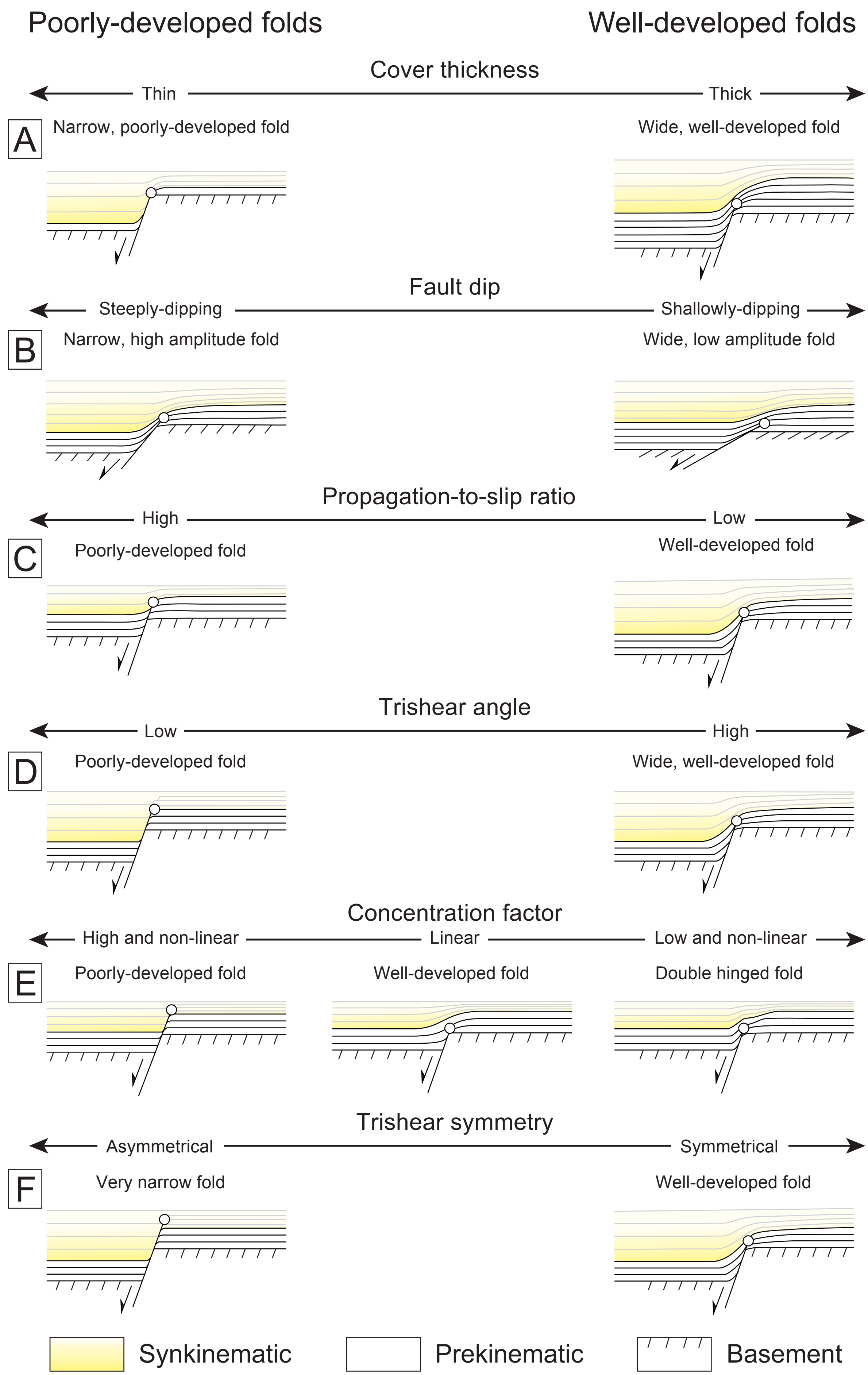

Poorly-developed folds
Well-developed folds
Cover thickness
Thin
Thick
A
Narrow, poorly-developed fold
Wide, well-developed fold
Fault dip
Steeply-dipping
Shallowly-dipping
B
Narrow, high amplitude fold
Wide, low amplitude fold
Propagation-to-slip ratio
High
Low
C
Poorly-developed fold
Well-developed fold
Trishear angle
Low
High
D
Poorly-developed fold
Wide, well-developed fold
Concentration factor
High and non-linear
Linear
Low and non-linear
E
Poorly-developed fold
Well-developed fold
Double hinged fold
Trishear symmetry
Asymmetrical
Symmetrical
F
Very narrow fold
Well-developed fold
Synkinematic
Prekinematic
Basement

Fig. 7

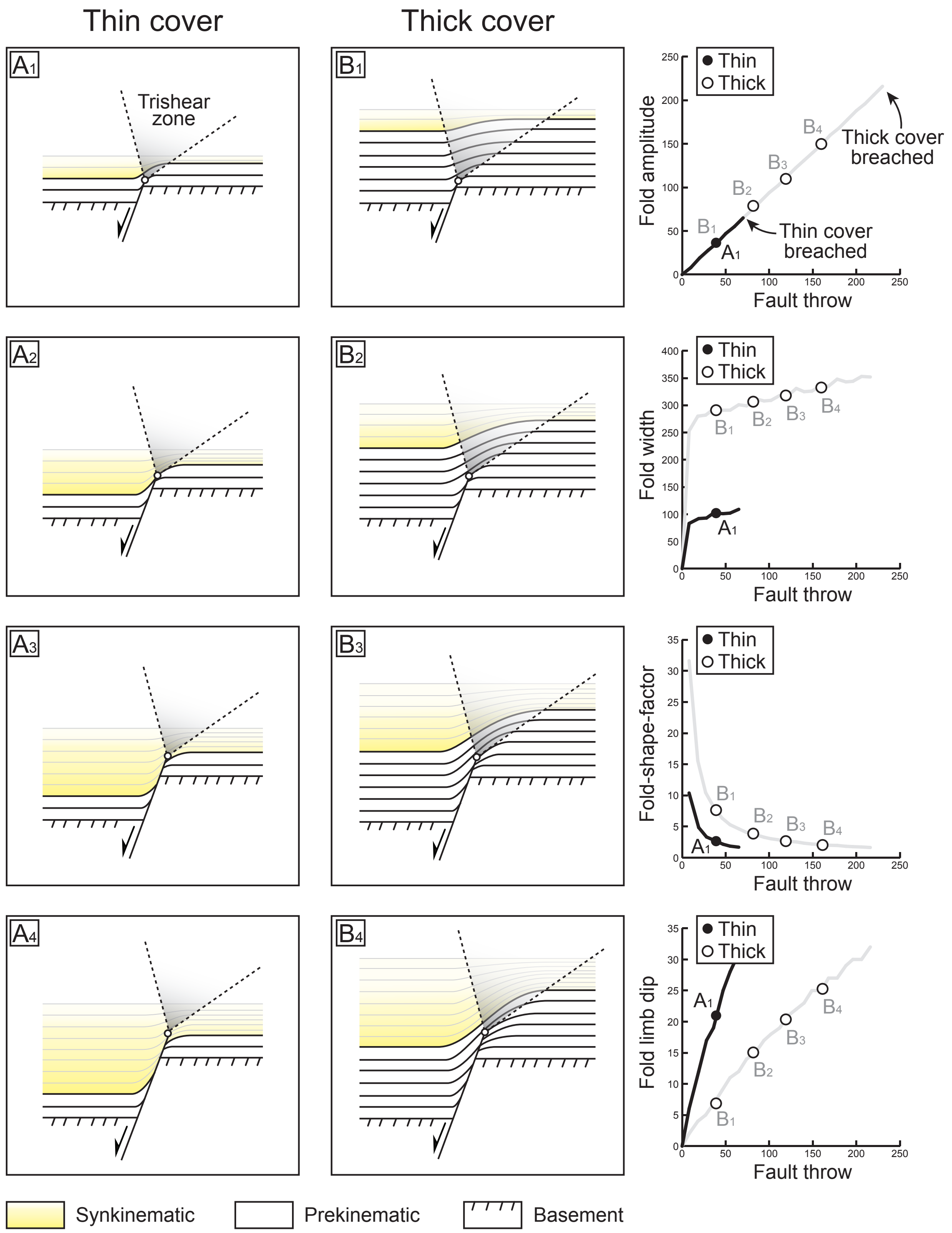

Thin cover
Thick cover
A1
Trishear zone
B1
Thin
Thick
Fold amplitude
Thick cover breached
Thin cover breached
Fault throw
A2
B2
Fold width
A3
B3
Fold-shape-factor
A4
B4
Fold limb dip
Synkinematic
Prekinematic
Basement

Fig. 8

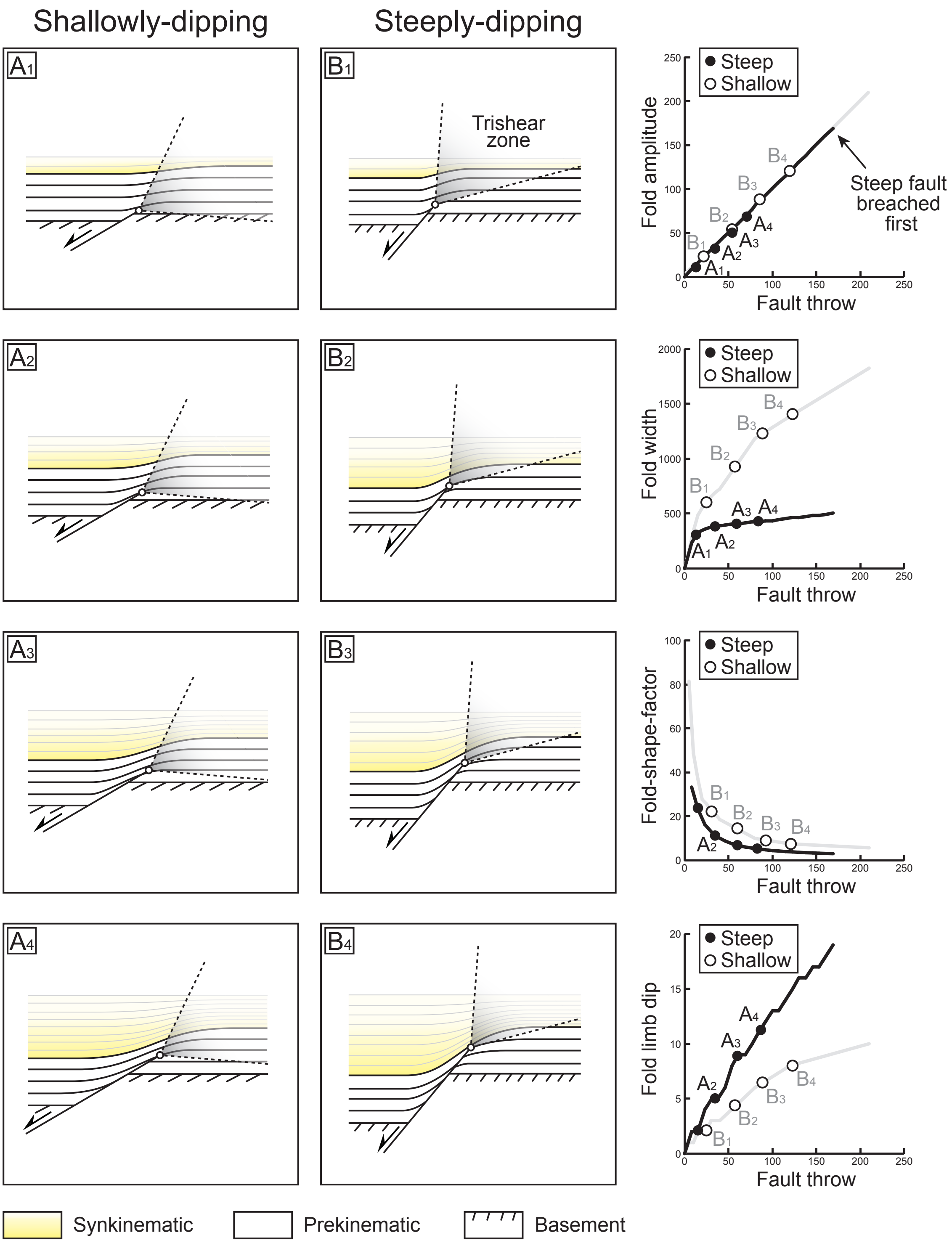

Shallowly-dipping
Steeply-dipping
A1
B1
Trishear zone
A2
B2
A3
B3
A4
B4
Steep
Shallow
Fold amplitude
Steep fault breached first
Fold width
Fold-shape-factor
Fold limb dip
Fault throw
Synkinematic
Prekinematic
Basement

Fig. 9

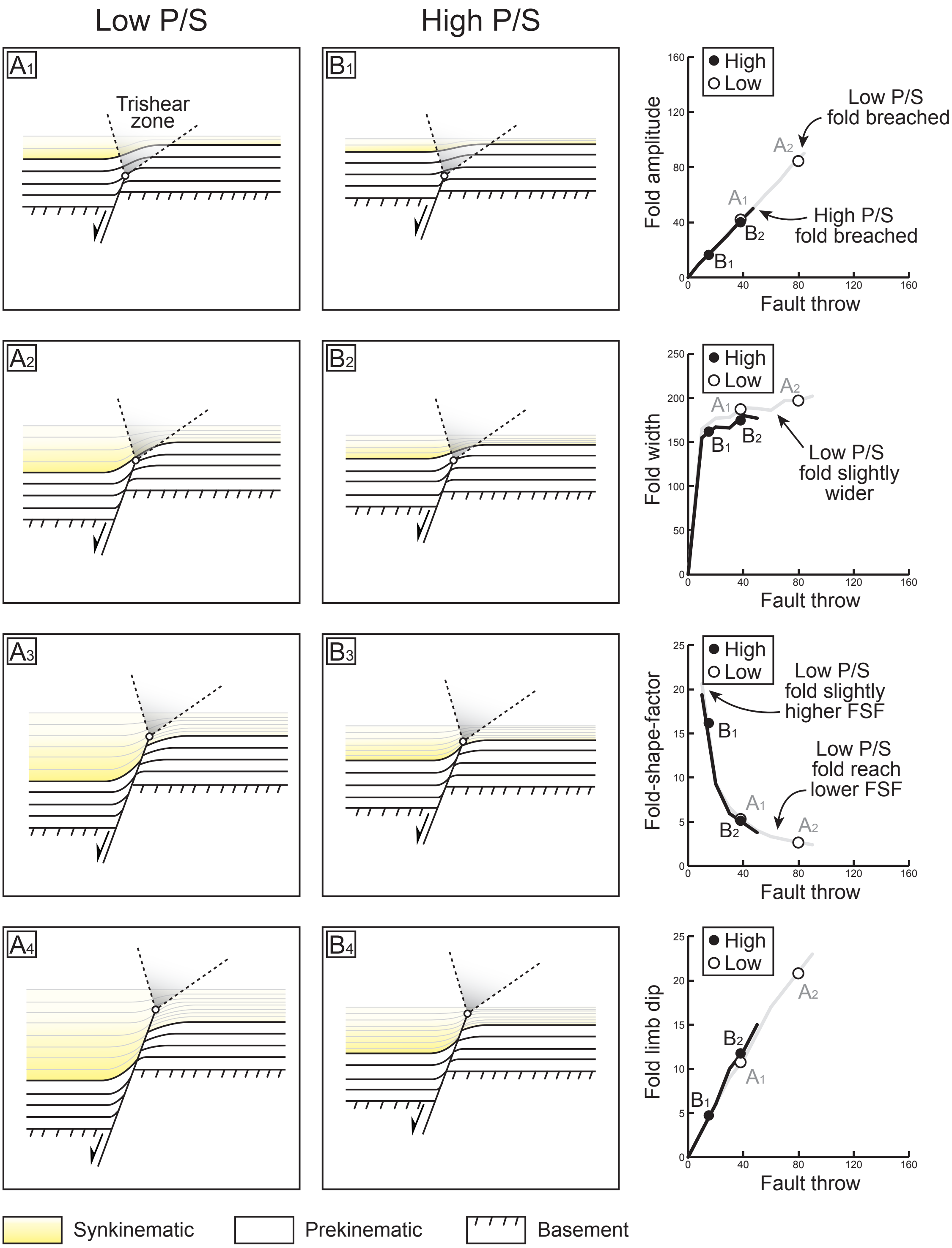

Low P/S
High P/S
A1
Trishear zone
B1
A2
B2
A3
B3
A4
B4
High
Low
Low P/S fold breached
High P/S fold breached
Fold amplitude
Fault throw
Fold width
Low P/S fold slightly wider
Fold-shape-factor
Low P/S fold slightly higher FSF
Low P/S fold reach lower FSF
Fold limb dip
Synkinematic
Prekinematic
Basement

Fig. 10

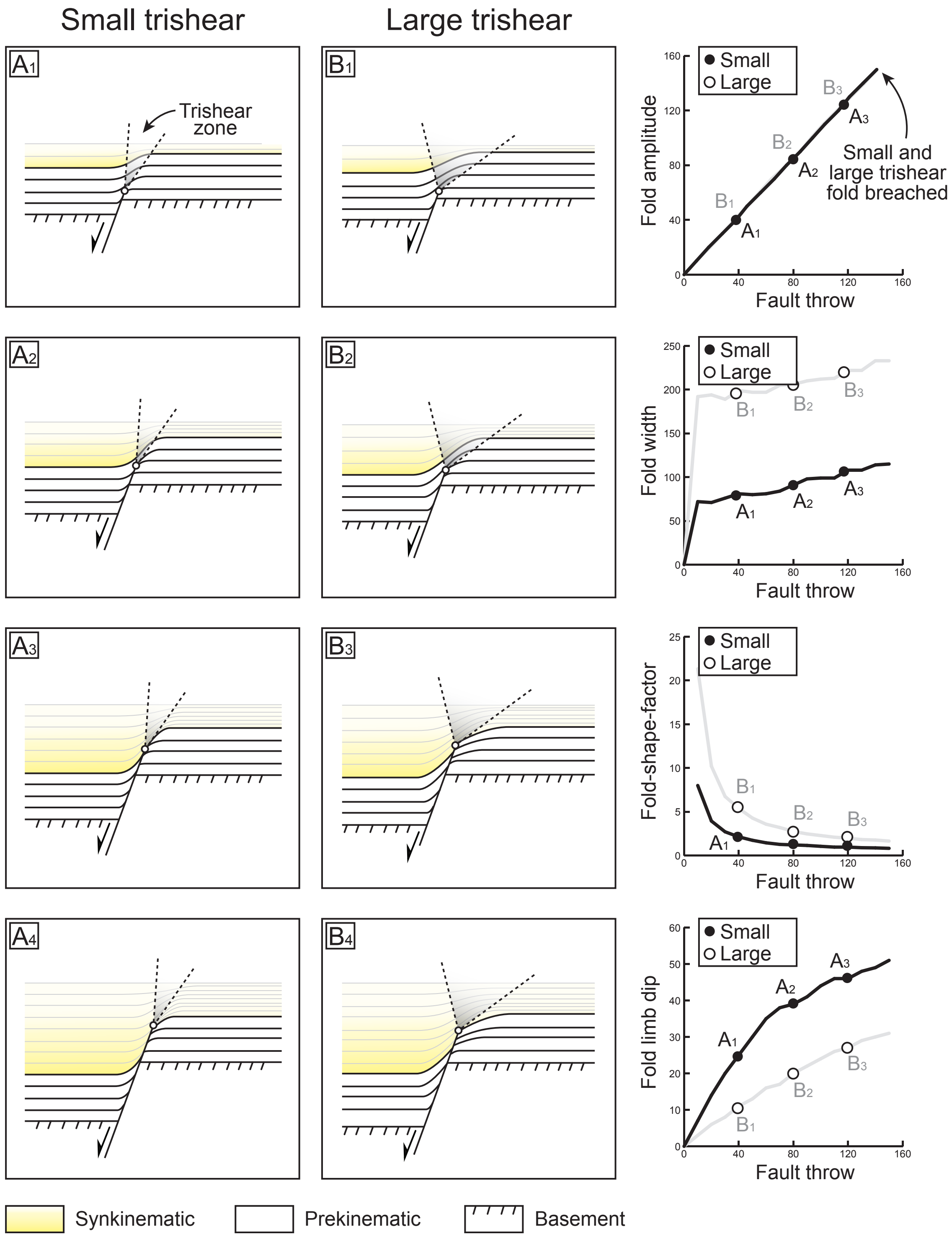

Small trishear
Large trishear
A1
B1
Trishear zone
Small
Large
Fold amplitude
Fault throw
Small and large trishear fold breached
A2
B2
Fold width
A3
B3
Fold-shape-factor
A4
B4
Fold limb dip
Synkinematic
Prekinematic
Basement

Fig. 11

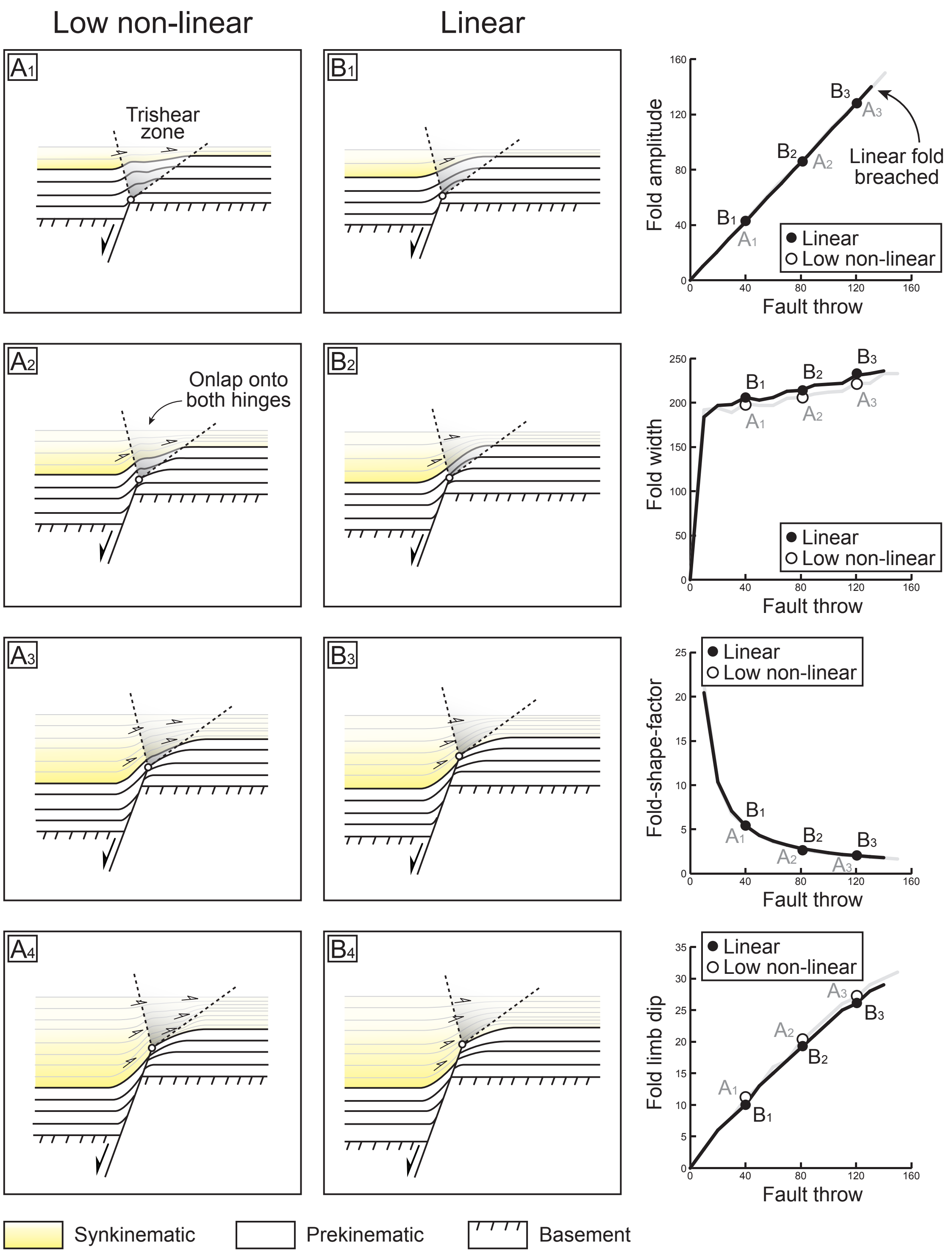

Low non-linear
Linear
A1
Trishear zone
B1
A2
Onlap onto both hinges
B2
A3
B3
A4
B4
Fold amplitude
Fault throw
Linear fold breached
Linear
Low non-linear
Fold width
Fold-shape-factor
Fold limb dip
Synkinematic
Prekinematic
Basement

Fig. 12

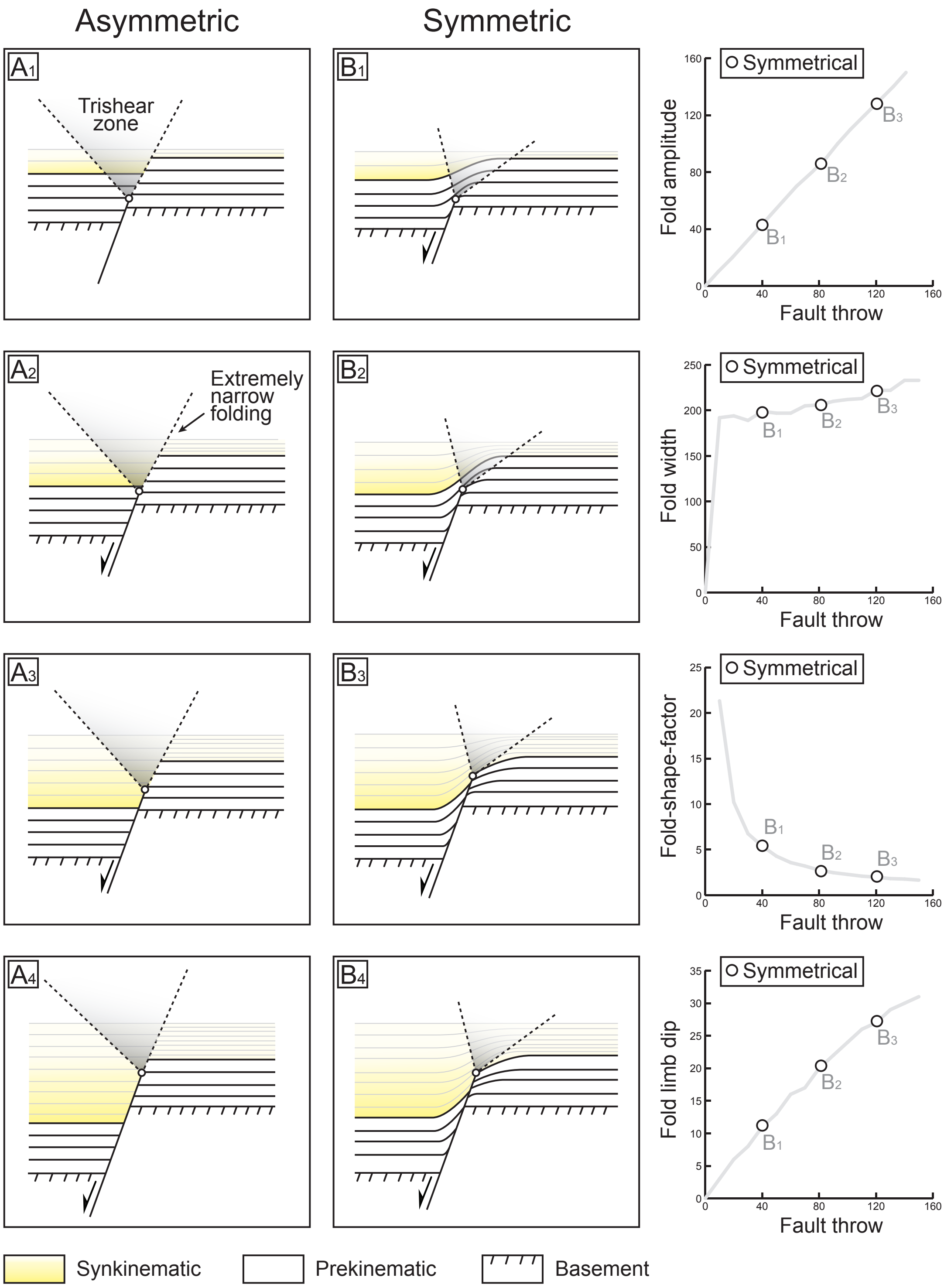

Asymmetric
Symmetric
A1
Trishear zone
B1
A2
Extremely narrow folding
B2
A3
B3
A4
B4
Symmetrical
Fold amplitude
Fold width
Fold-shape-factor
Fold limb dip
Fault throw
Synkinematic
Prekinematic
Basement

Fig. 13

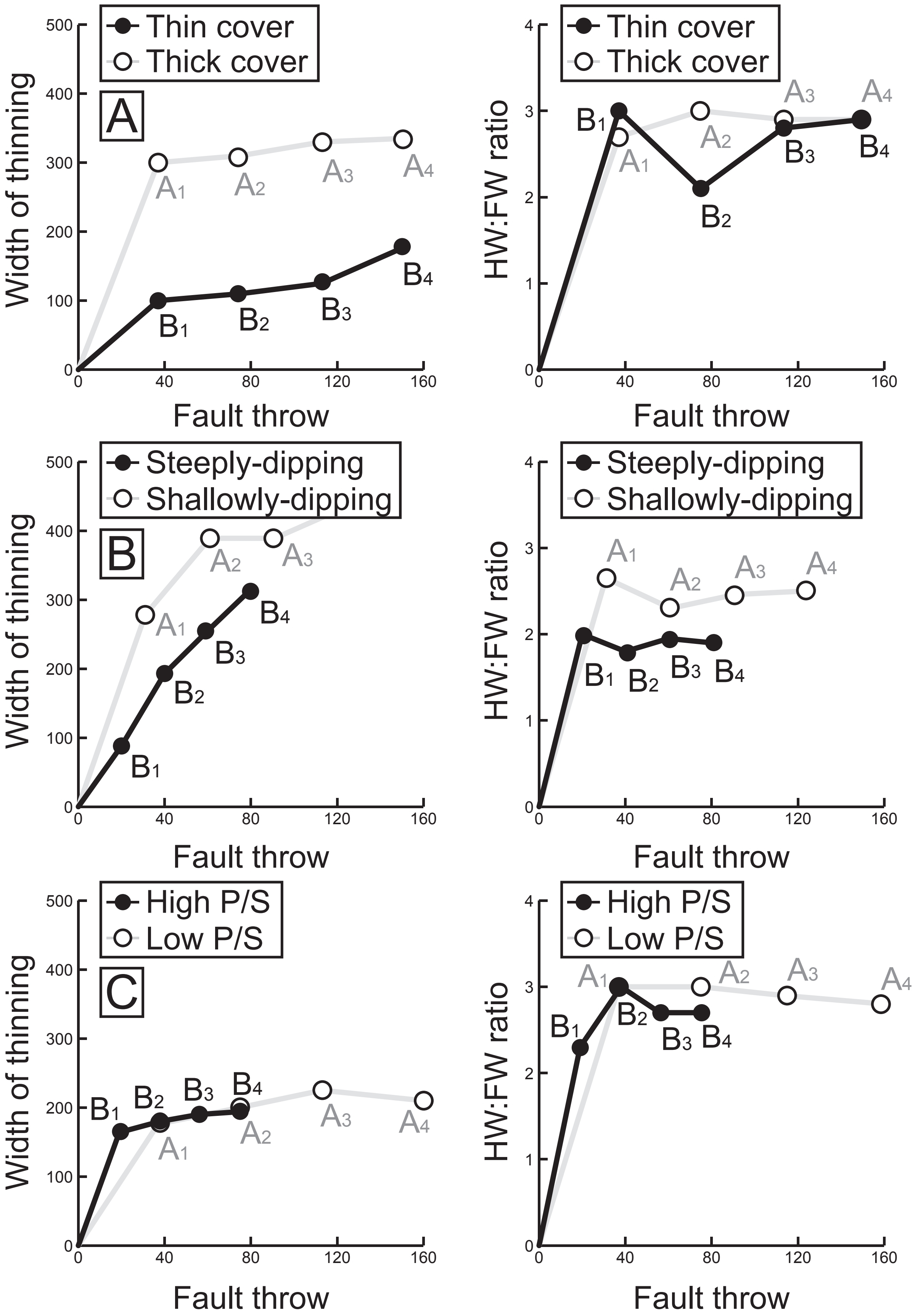

Thin cover
Thick cover
A
Width of thinning
Fault throw
HW:FW ratio
Steeply-dipping
Shallowly-dipping
B
High P/S
Low P/S
C

Fig. 13 (contd.)

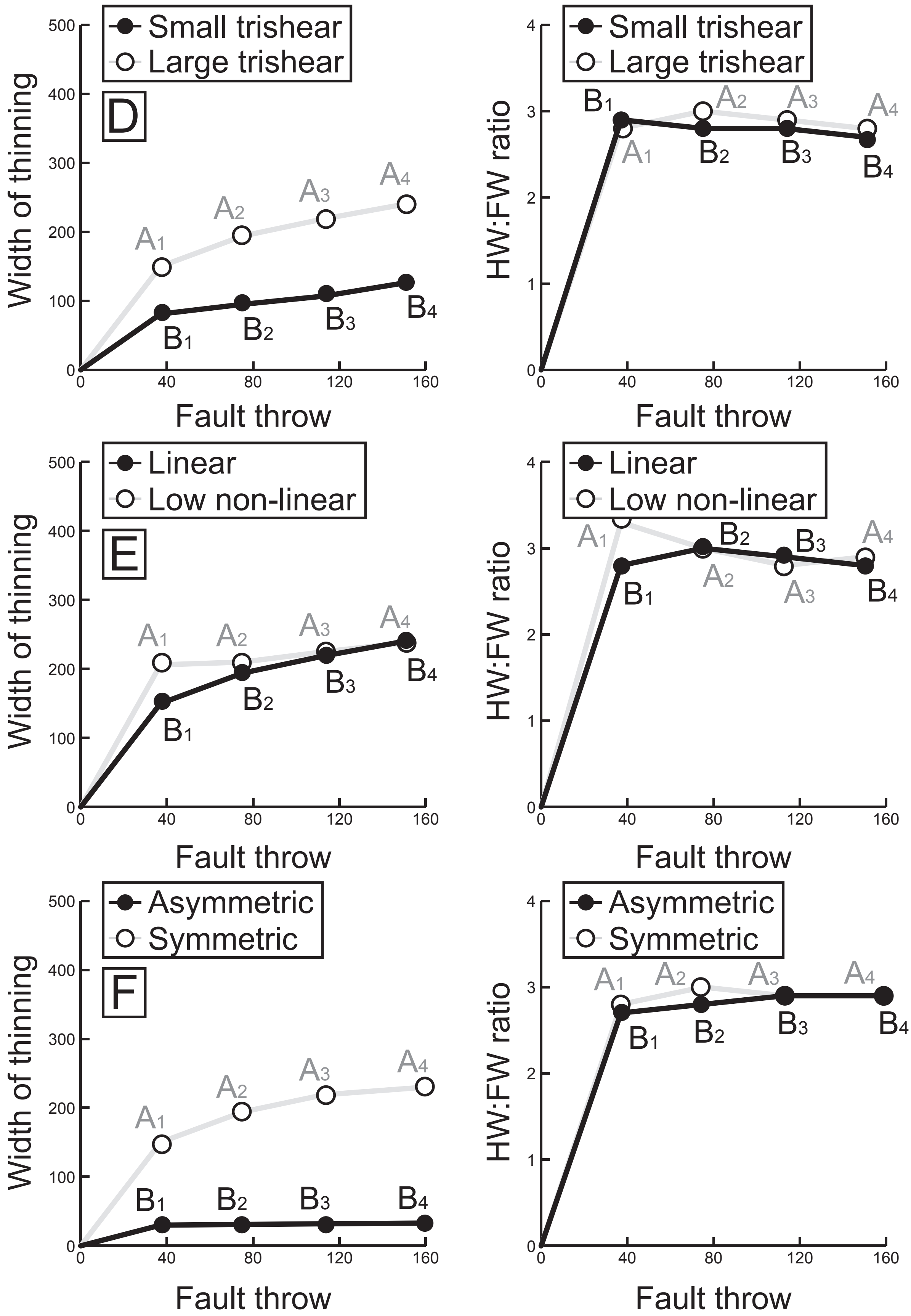

Small trishear
Large trishear
D
Width of thinning
Fault throw
HW:FW ratio
Linear
Low non-linear
E
Asymmetric
Symmetric
F

Fig. 14

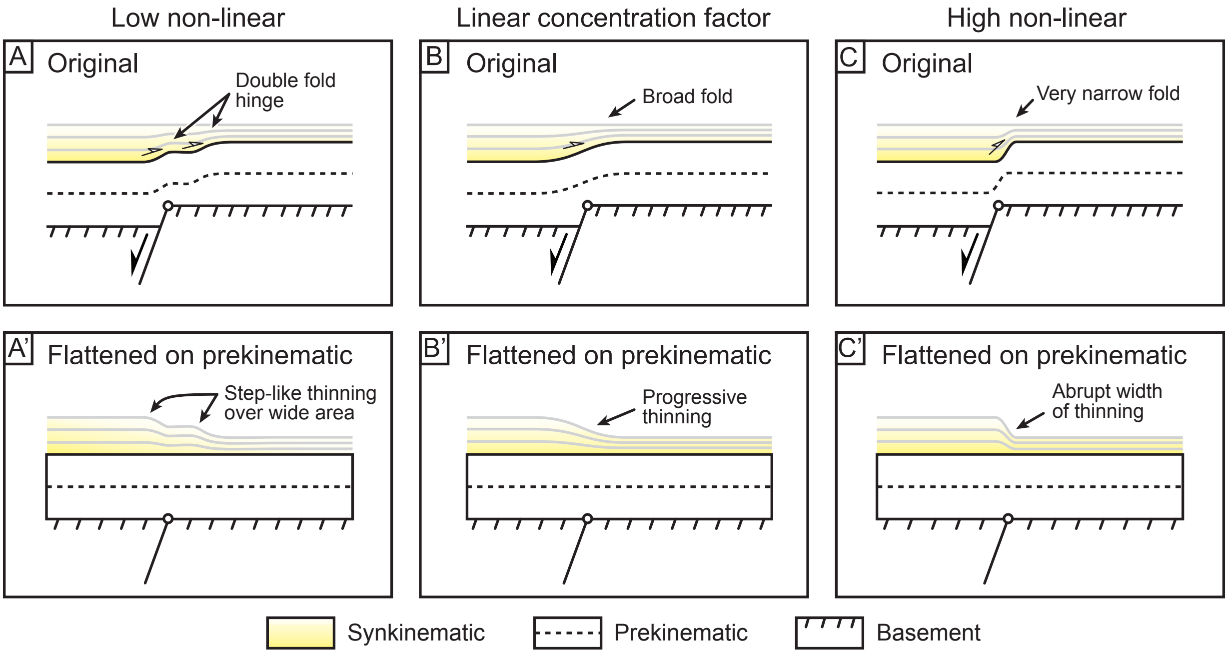
Low non-linear
Linear concentration factor
High non-linear
A
Original
Double fold hinge
B
Original
Broad fold
C
Original
Very narrow fold
A'
Flattened on prekinematic
Step-like thinning over wide area
B'
Flattened on prekinematic
Progressive thinning
C'
Flattened on prekinematic
Abrupt width of thinning
Synkinematic
Prekinematic
Basement

Fig. 15

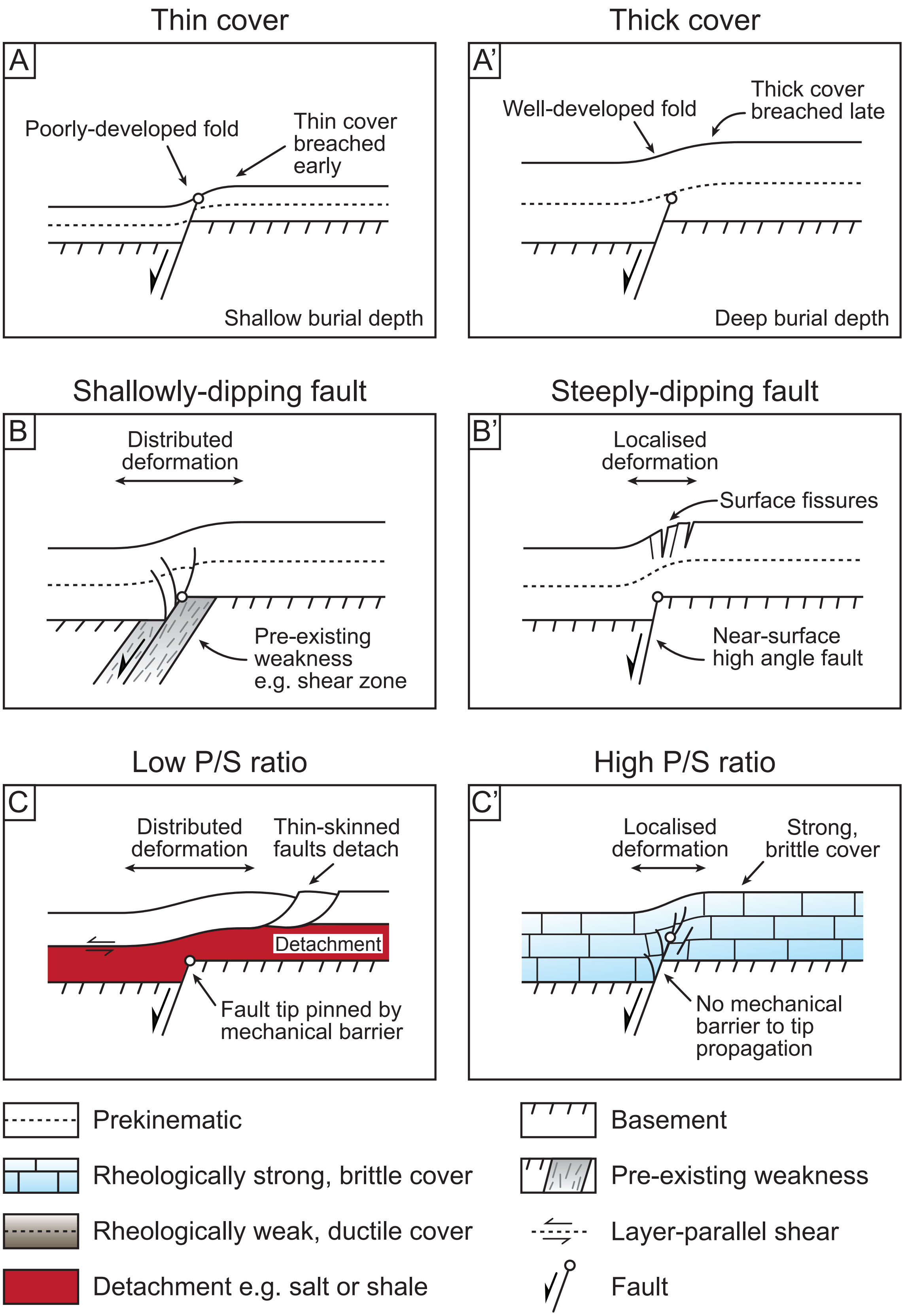

Thin cover
A
Poorly-developed fold
Thin cover breached early
Shallow burial depth
Thick cover
A'
Well-developed fold
Thick cover breached late
Deep burial depth
Shallowly-dipping fault
B
Distributed deformation
Pre-existing weakness e.g. shear zone
Steeply-dipping fault
B'
Localised deformation
Surface fissures
Near-surface high angle fault
Low P/S ratio
C
Distributed deformation
Thin-skinned faults detach
Detachment
Fault tip pinned by mechanical barrier
High P/S ratio
C'
Localised deformation
Strong, brittle cover
No mechanical barrier to tip propagation
Prekinematic
Basement
Rheologically strong, brittle cover
Pre-existing weakness
Rheologically weak, ductile cover
Layer-parallel shear
Detachment e.g. salt or shale
Fault

Fig. 15 (contd)

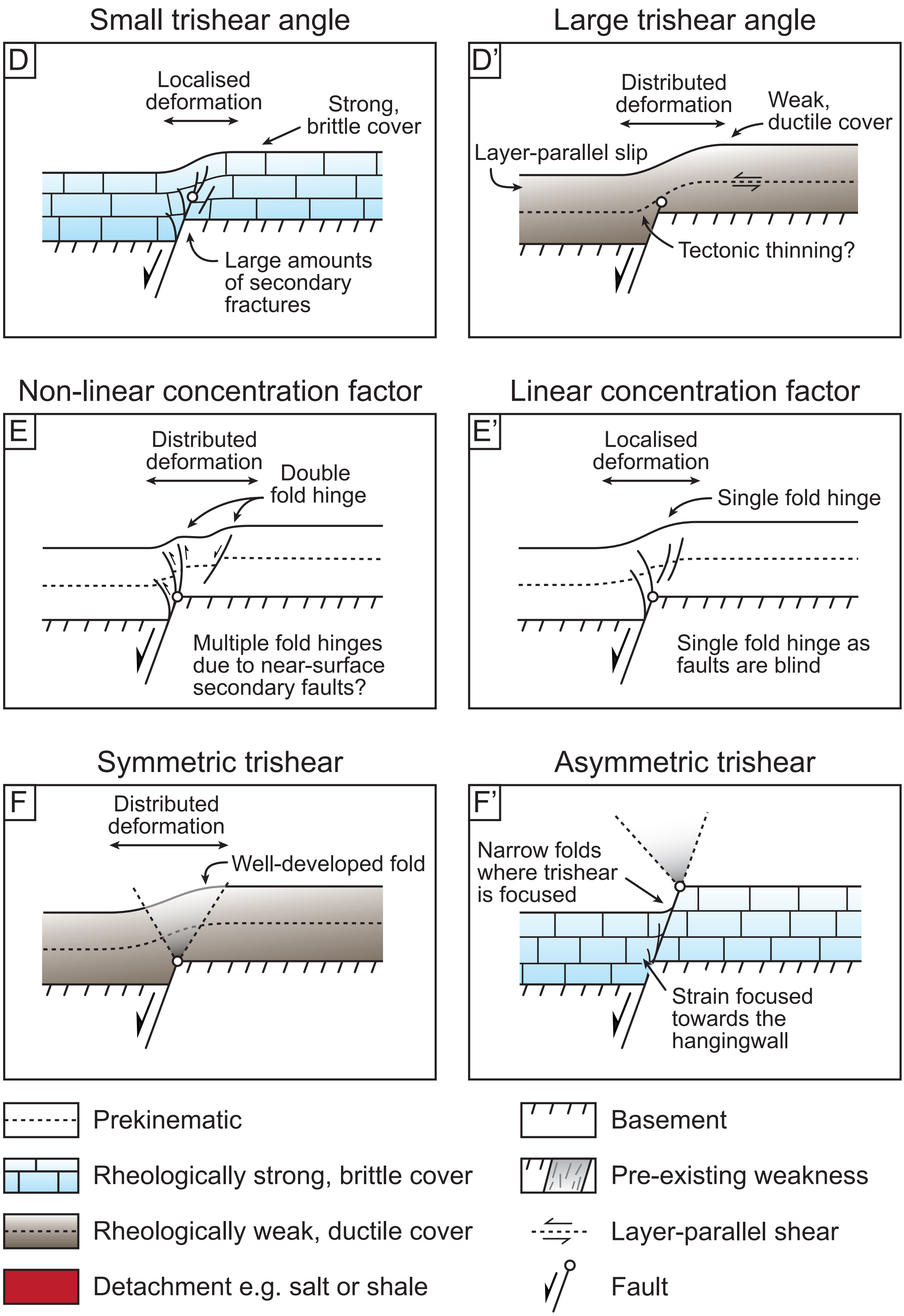

Small trishear angle
D
Localised
deformation
Strong,
brittle cover
Large amounts
of secondary
fractures
Large trishear angle
D'
Distributed
deformation
Weak,
ductile cover
Layer-parallel slip
Tectonic thinning?
Non-linear concentration factor
E
Distributed
deformation
Double
fold hinge
Multiple fold hinges
due to near-surface
secondary faults?
Linear concentration factor
E'
Localised
deformation
Single fold hinge
Single fold hinge as
faults are blind
Symmetric trishear
F
Distributed
deformation
Well-developed fold
Asymmetric trishear
F'
Narrow folds
where trishear
is focused
Strain focused
towards the
hangingwall
Prekinematic
Rheologically strong, brittle cover
Rheologically weak, ductile cover
Detachment e.g. salt or shale
Basement
Pre-existing weakness
Layer-parallel shear
Fault

Fig. 16

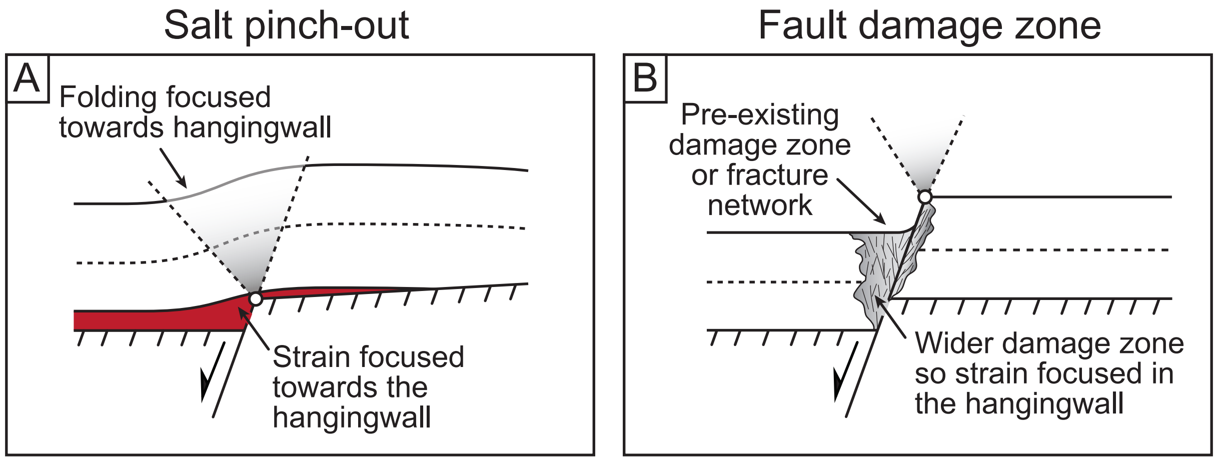

Salt pinch-out
A
Folding focused towards hangingwall
Strain focused towards the hangingwall
Fault damage zone
B
Pre-existing damage zone or fracture network
Wider damage zone so strain focused in the hangingwall

Table 1

Example	Fault dip	Trishear angle	Propagation-to-slip ratio (P/S)	Trishear symmetry	Maximum cover thickness	Reference
Clay model; Withjack et al., 1990	75	40*	-0.3*	Asymmetrical (68% towards footwall)*	5 cm*	Allmendinger, 1998
Clay model; Withjack et al., 1990	75	80	-1.5	Symmetrical	5 cm	Hardy and McClay, 1999
Hamadat Monocline, Gulf of Suez	65	120	-1 to -0.1	Symmetrical	690 m	Khalil and McClay, 2002
Mechanical model	90	32	-3	Symmetrical	10 km	Cardozo et al., 2003
Clay model	60	70	-4 to -1	Asymmetrical (55% towards footwall)	6 cm	Jin and Groshong, 2006
Clay Model	90	70	-3 to 0	Asymmetrical (60% towards footwall)	6 cm	Jin and Groshong, 2006
Gulf of Suez from Withjack et al., 1990	67	50	-2 to -1.2	Asymmetrical (54% towards hangingwall)	1500 m	Jin and Groshong, 2006
Southern Vorges Fault Zone, Rhine Graben	70	120	-3 to 0	Asymmetrical (60% towards hangingwall)	350 - 400 m	Ford et al., 2007
Guebwiller Fault Zone, Rhine Graben	70	120	-3 to 0	Asymmetrical (60% towards hangingwall)	450 – 900 m	Ford et al., 2007
Illfurth Fault Zone, Rhine Graben	70	120	-1 to 0	Asymmetrical (60% towards hangingwall)	350 – 500 m	Ford et al., 2007

Table 1 (contd)

Example	Fault dip	Trishear angle	Propagation-to-slip ratio (P/S)	Trishear symmetry	Maximum cover thickness	Reference
Gilbertown Graben	60 - 52	60	-40 to -6	Asymmetrical (58% towards hangingwall)	700 m	Jin et al., 2009
Hadahid Fault Zone, Gulf of Suez	77	81	1.89	Symmetrical	300 m	Cardozo et al., 2011
Hadahid Fault Zone, Gulf of Suez	71	99	1.87	Symmetrical	360 m	Cardozo et al., 2011
Hadahid Fault Zone, Gulf of Suez	69	62	1.9	Symmetrical	300 m	Cardozo et al., 2011
Hadahid Fault Zone, Gulf of Suez	75	64	1.43	Symmetrical	360 m	Cardozo et al., 2011
Hadahid Fault Zone, Gulf of Suez	80	22	0.75	Symmetrical	460 m	Cardozo et al., 2011
Clay model from Withjack et al., 1990	70 - 75	40 - 50	-2.25 to -1.234	Symmetrical	5 cm	Cardozo et al., 2011
Clay model from Withjack et al., 1990	72	50 - 70	-2	Symmetrical	5 cm	Cardozo et al., 2011
Clay model from Withjack et al., 1990	73 - 75	40 - 80	-1.75 to -2.25	Symmetrical	5 cm	Cardozo et al., 2011
Clay model from Withjack et al., 1990	75	30 - 70	-1.75 to 2.0	Symmetrical	5 cm	Cardozo et al., 2011

Table 2

Model number	Prekinematic cover thickness	Fault dip	Trishear angle	Propagation-to-slip ratio (P/S)	Trishear symmetry	Concentration factor	Figure number
1	2 units	70	50	0.5	Symmetrical	1 (linear)	4.7; 4.13A
2	6 units	70	50	0.5	Symmetrical	1 (linear)	4.7; 4.13A
3	4 units	30	50	0.5	Symmetrical	1 (linear)	4.8; 4.13B
4	4 units	50	50	0.5	Symmetrical	1 (linear)	4.8; 4.13B
5	4 units	70	50	1	Symmetrical	1 (linear)	4.9; 4.13C
6	4 units	70	50	2	Symmetrical	1 (linear)	4.9; 4.13C
7	4 units	70	30	0.5	Symmetrical	1 (linear)	4.10; 4.13D
8	4 units	70	70	0.5	Symmetrical	1 (linear)	4.10; 4.13D
9	4 units	70	50	0.5	Symmetrical	0.5 (non-linear)	4.11; 4.13E;
10	4 units	70	50	0.5	Symmetrical	1 (linear)	4.11; 4.13E;
11	4 units	70	50	0.5	Symmetrical	1 (linear)	4.12; 4.13F
12	4 units	70	50	0.5	Asymmetrical	1 (linear)	4.12; 4.13F